SAND--95-2528

12-11-95

CONTRACTOR REPORT

SAND95–2528
Unlimited Release
UC–1272

Solar Kinetics' Photovoltaic Concentrator Module and Tracker Development

David L. White and Bennett Howell
Solar Kinetics, Inc.
10635 King William Drive
Dallas, TX 75220

Prepared by Sandia National Laboratories Albuquerque, New Mexico 87185
and Livermore, California 94550 for the United States Department of Energy
under Contract DE-AC04-94AL85000

Printed November 1995

Issued by Sandia National Laboratories, operated for the United States Department of Energy by Sandia Corporation.

Available to DOE and DOE contractors from
Office of Scientific and Technical Information
PO Box 62
Oak Ridge, TN 37831

Prices available from (615) 576-8401, FTS 626-8401

Available to the public from
National Technical Information Service
US Department of Commerce
5285 Port Royal Rd
Springfield, VA 22161

NTIS price codes
Printed copy: A04
Microfiche copy: A01

Distribution
Category UC-1272

SAND95-2528
Unlimited Release
Printed November 1995

Solar Kinetics' Photovoltaic Concentrator Module and Tracker Development

David L. White and Bennett Howell
Solar Kinetics, Inc.
10635 King William Drive
Dallas, Texas 75220

Sandia Contract 40-8941B

ABSTRACT

Solar Kinetics, Inc., has been developing a point-focus concentrating photovoltaic module and tracker system under contract to Sandia National Laboratories. The primary focus of the contract was to achieve a module design that was manufacturable and passed Sandia's environmental testing. Nine modules of two variations were assembled, tested, and characterized in Phase I, and results of these tests were promising, with module efficiency approaching the theoretical limit achievable with the components used. The module efficiency was 11.9% at a solar irradiance of 850 W/m^2 and an extrapolated cell temperature of 25°C. Improvements in module performance are anticipated as cell efficiencies meet their expectations. A 2-kW tracker and controller accommodating 20 modules was designed, built, installed, and operated at Solar Kinetics' test site. The drive used many commercially available components in an innovative arrangement to reduce cost and increase reliability. Backlash and bearing play were controlled by use of preloaded, low slip-stick, synthetic slide bearings. The controller design used a standard industrial programmable logic controller to perform ephemeris calculations, operate the actuators, and monitor encoders.

Executive Summary

The significant technical progress achieved by Solar Kinetics, Inc. (SKI) in developing a point-focus concentrating photovoltaic (PV) module and tracking array is described. This work was funded jointly by SKI and the U. S. Department of Energy as part of the PV Concentrator Initiative Program. Work Completed during two of the planned three phases of the development effort are discussed. The contract was ended due to a funding shortfall for the Concentrator Initiative Program. Two generations of modules and a 2-kW tracking array were designed and fabricated by SKI. Sandia National Laboratories, manager of the contract with SKI, provided technical assistance and component testing for SKI.

SKI's modules use injection-molded acrylic Fresnel lenses to focus sunlight onto 24 single-crystal silicon cells. The high concentration ratio (282X geometric) significantly reduces the area of the expensive silicon cell while achieving a high efficiency. Module efficiency was 11.9% (at a peak rating condition of 850 W/sq.m insolation and 25 °C cell temperature) using cells with a peak efficiency of over 17%. This is near the limit of efficiency achievable by the low-cost optics. Higher efficiencies can be obtained using higher efficiency cells which are available at over 19% efficiency. The module housing was constructed of aluminum for durability, high heat rejection, and ease of manufacturing. Its dimensions were nominally 85 inches (2.16m) long, 15 inches (0.38m) wide and 10 inches (0.25m) deep.

A significant portion of the program was devoted to developing solder bond processes that provided good initial bond quality (as determined by radiographic and ultrasound imaging) and could reliably pass Sandia's accelerated thermal and humidity/freeze environmental cycle tests. Excellent initial bond quality was achieved using solder paste by the time the technical effort was ended. Progress was made in surviving the Sandia environmental cycle tests. Cell assemblies exhibited minimal reductions in efficiency following 250 thermal cycles, but failed the test specifications due to lot average void area increases greater than 10%. Failure of the humidity cycling test was identified as being caused by oxidizing of the cell aluminum metallization layer, requiring changes at the cell manufacturing level.

A 2-kW tracker and controller accommodating 20 modules was designed, built, installed, and successfully operated at SKI's test site. The drive used many commercially available components in an innovative arrangement to reduce cost and increase reliability. Backlash and bearing play were controlled by use of preloaded, low slip-stick, synthetic slide bearings. The controller design used a standard industrial programmable logic controller to perform ephemeris calculations, operate the actuators, and monitor encoders.

Table of Contents

List of Figures

List of Tables

1.0 Summary

This is the final report of product development of a commercial photovoltaic concentrator module and tracking system. The project was performed under the Department of Energy Photovoltaic Concentrator Initiative Program. The work was a cost-shared effort between the U.S. Department of Energy and Solar Kinetics, Inc. (SKI). SNL National Laboratories (SNL), Albuquerque, NM, was the liaison for the project under contract #40-8941B.

This program was being performed in three sequential phases. The first phase was 15 months, and the following two phases were to be 20 months each. Project activities were initiated in October 1990, the Phase I activities were concluded in January 1992, and Phase II activities were terminated in March 1993.

The final objective for all phases of this work was the development of a low-cost, point-focus, concentrator module for commercial applications. Detailed design and performance analyses of various components and subsystems were performed in Phase I. The two key subsystems were the PV cell assembly and the concentrator module. These subsystems were designed in detail, fabricated, and evaluated at SKI.

A key emphasis of Phase I was the development of environmentally survivable cell assemblies and modules (1). The cell assemblies and modules were required to pass qualification tests for photovoltaic concentrators established by Barlow and Richards (2). These evaluation tests, currently being revised by SNL, were established to screen hardware designs for susceptibility to known failure mechanisms. The qualification tests characterized electrical performance, safety, structural stability, and module integrity in response to accelerated environmental cycling. Modules and cell assemblies in future phases were to be subjected to additional testing as SNL continued to update photovoltaic evaluation criteria.

The module development was based on the 282-sun (geometric concentration) PV concentrator designed by SKI under a previous contract (3); some changes were incorporated in the Phase I design. Twenty-four point-focus Fresnel lenses were mounted as parquets above the cell assemblies. The cell assemblies, placed in two rows of twelve, were connected in series to obtain summation of voltages generated by all twenty-four assemblies. The electrical current generated by the module is dictated by the cell assembly with the smallest output. The assemblies were matched, based on output current at the maximum power point, to maximize the power yield from a module.

The modules were designed in two iterations during Phase I. Two Type-I modules were fabricated with a 2 x 6 lens parquet. This module had a single center lens partition clip between the two parquets. Bulkheads, designed to reduce module deflection under wind loads, were placed at alternate lenses.

One Type-I module was delivered to SNL for environmental and performance evaluation.

Moisture was absorbed by the acrylic lens during humidity/freeze evaluation test cycle. The corresponding expansion resulted in lens distortion. Moisture soak tests at SKI showed similar results.

The module was redesigned with six 2 x 2 Fresnel lens parquets separated by five lens partition clips. This modification was incorporated to minimize the distortion observed in the lenses as a result of the humidity/freeze cycling of the modules. The length of the Type-II module was greater due to the additional lens partition clips. The additional lens partition clips increased the stiffness of the module. The bulkheads were eliminated in the Type-II design.

The Type-II modules were not evaluated with the humidity/freeze cycle during Phase I. Solar Kinetics anticipated that the design change would limit lens distortion to an acceptable amount. Some improvement in electrical performance was also expected because the smaller parquets improved the ability to align the lens and cell assembly.

Extensive evaluation and selection of component materials and fabrication processes were conducted in Phase I. Materials and processes were evaluated based on prototype and production requirements. All module components, with the exception for the PV cell and lens, were designed by Solar Kinetics, Inc. Precision sheet metal parts were fabricated at SKI. All soldering processes were also developed at SKI facilities.

This effort established the various process control issues associated with the manufacture of each component. For the housing, these issues included material hardness, material thickness, dimensional fabrication tolerances, and ease of fabrication. A host of soldering variables were also defined during Phase I.

The final task performed in Phase I was the design and fabrication of a tracking platform. The first iteration was based on a polar drive configuration for a 1 kW array of modules. Development of this initial approach progressed to a structural layout, hybrid control flow chart, and a shadow-band sun sensor. Detailed investigation concerning the ability of this tracker for scale-up to a 20 kW configuration revealed geometric constraints. The 20 kW array would have to be an immense structure to accommodate tracking about the polar axis. Therefore, alternate tracker concepts were evaluated.

The tracking concept chosen in Phase I was an azimuth/elevation (Az/El) "open loop" control design. This subsequent design can be scaled for larger arrays for larger power capacity per drive. The "open loop" control system eliminated the requirement for a shadow-band sun sensors. SKI designed and fabricated a 2 kW (20 modules) Az/El tracking drive and controller in Phase I. The tracking platform was operated in the SKI fabrication facility for initial testing of the

hardware and the control logic. The tracker was installed at the SKI test site in Dallas during Phase II.

This report summarizes the work completed up to the date the contract was terminated in the middle of Phase II. The report is divided into the following sections: 2.0 Phase I Results; 3.0 Phase II Results; 4.0 Commercial Markets; 5.0 Conclusions; and 6.0 References.

2.0 Phase I Results

The first phase in development of a point-focus concentrating PV module was a success. Cell assembly and module fabrication issues were addressed by utilizing cost-effective materials and defining low-cost manufacturing methods. Material costs were minimized, although processing and assembly cost evaluation were an ongoing task in the contract.

2.1 Description Of Cell Assembly Components

The solar cell assembly developed in Phase I consisted of five components: the solar cell, heat spreader, bottom contact tab, top contact, and the secondary optical element. An exploded view of the cell assembly is shown in Figure 2.1. The function of each component is described below.

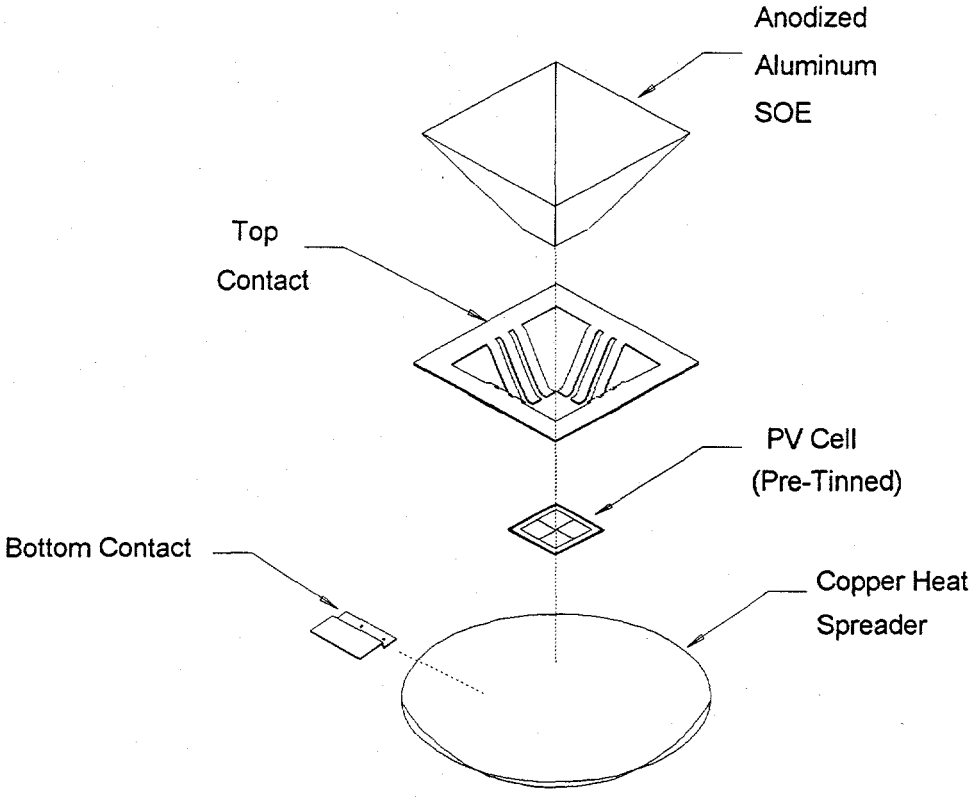

Figure 2.1 Concentrating Photovoltaic Cell Assembly Components

A solar cell is a photovoltaic (PV) semiconductor device that converts solar radiation into usable electrical energy. Solar flux that is not converted to electricity and not reflected is dissipated as heat. The photovoltaic cell used in Phase I was an N+ on P/P+ type single crystal silicon cell with efficiencies varying from 15% to 19% at 300X and 25 °C. Detailed specifications for this PV cell, manufactured by the Applied Solar Energy Corporation (ASEC), is included as Appendix A of the Phase I report (1). The PV cell had an active area of 0.165 (0.406 x 0.406) square inches. A current-carrying metallized bus bar along the periphery of the PV cell increased the overall size to 0.294 (0.542 x 0.542) square inches. The cell thickness was approximately 0.008 inches.

The solar cells supplied by ASEC and used for Phase I had layers of various compatible metals deposited on the back to achieve a solderable surface. The final metallized layer on the cell was silver. Prior to soldering of the cell, the cell back was cleaned and the surface prepared for pretinning.

The heat spreader was a 2.5-inch diameter copper disk used for dissipating heat generated at the PV cell. The disk had notches diametrically opposed on the 2.5 inch circle diameter. The location of these notches was accurate within ± 0.002 inch.

The copper alloy was 102, oxygen-free, high-conductivity copper (OFHC). This alloy, a pure, oxygen-free copper, was selected because of its good solderability. The high electrical conductivity of 102 copper also minimizes resistive loss in the cell assembly.

The heat spreader functioned as a heat dissipater and "spreader" for solar flux not converted into electricity or reflected at the cell. Heat transfer analysis software, written at SNL, was used for the design of the heat spreader. The software simulated the various layers between the solar cell and the housing. The heat spreader was designed to keep the cell temperature low. A 0.06% cell efficiency loss was predicted for every 1 °C rise in cell temperature. Under typical operating weather conditions, the software predicted a cell temperature of 65 °C (150 °F) given the module and spreader design developed in Phase I.

The bottom contact tab was also fabricated from 102 copper. The offset in the tab, as shown on Figure 2.1, reduced the heat transferred from the interconnect to the cell assembly during soldering. The offset also defined the bonding area between the spreader and the tab.

The solar cell and bottom contact tab were soldered to the heat spreader. The interconnect assembly was soldered to the bottom contact tab and not to the heat spreader to avoid reflow in the cell solder joints.

Five punched holes were located in the bonding area of the tab to vent flux that is trapped during soldering and prevent voids in the solder. These holes also served as a means for a qualitative inspection, since a lack of solder within the holes indicates insufficient solder in the bond.

The top contact functioned as the positive lead of the PV cell assembly. Small fingers extended to the PV cell and were soldered to the metallized cell bus bar around the perimeter of the solar cell. The contact was designed with two fingers per side for a total of eight fingers. An S-shaped stress relief bend was provided in each finger that terminated with a 0.144 x 0.044 inch pad.

The angled fingers of the top contact provided the structural support for the secondary optical element (SOE). The top contact fingers were slanted at an angle approximately equal to the angle of the SOE. This slant provided the maximum bonding area for adhering the SOE to the top contact.

A 0.5 x 1.0 inch tab extended from one side of the top contact to provide a surface for bonding to the electrical interconnect strap. This extension also reduced the heat transferred to the cell during interconnect soldering by increasing the thermal conductivity path.

The SOE, a reflective cone mounted on the top of the cell assembly, was used to collect and focus stray solar flux onto the cell. This element reduced the effects of errors such as lens misalignment and off-axis tracking. The SOE also improved the uniformity of flux distribution by reflecting energy to areas of the cell with otherwise low flux density.

Chemically polished specular aluminum with a total reflectivity of 88% was used for the SOE. This element was stamped and folded at SKI using a tab-in-slot technique at the corner.

The SOE cone angle was optimized for maximum solar cell efficiency using lens optics utilities software written by James Associates of Boulder, Colorado. The optimized included cone angle was approximately 60 degrees. The concentration ratio for the cone was approximately 15 to 1.

A double-sided foam adhesive was used for bonding the SOE to the cell assembly. Small strips were placed on the outside of the SOE near the exit aperture. The SOE was then attached to the top contact fingers. A gap of approximately 0.020 inch was maintained between the solar cell and SOE.

2.1.1 Solders and Fluxes

Solders were used in various locations within the cell assembly and the PV module. Within the cell assembly, solder was used for attaching the solar cell to the heat spreader. Solder was also used for connecting the top contact fingers to the PV cell bus bar. Likewise, the bottom contact tab was soldered to the heat spreader. Within the module, solder was used to attach the electrical interconnects to the cell assemblies and diodes.

Several design and fabrication constraints were considered in all module solder joints. A solder bond provided the path for electrical current from the positive and negative sides of the solar cell assembly. The solder in the cell attachment bond also acted as a thermal conductor under the solar cell. Large voids in the solder bond under the cell impede the thermal path and result in high

temperatures and low cell efficiencies. Small voids are a means for crack initiation and propagation through the solder from thermal fatigue loads. Therefore, the need for a void-free or low void solder bond was critical to optimum cell performance. Other solder locations provided structural support as well as electrical continuity. Coefficient of thermal expansion (CTE) mismatch between solders, copper, and the PV cell resulted in thermal stresses that all bonded joints must withstand.

Several types of solders and fluxes were used within the module. During earlier efforts, different solder alloys were evaluated to achieve optimum bond results. Later, a single solder was used for all bonds within the cell assembly and module. This solder was available in sheet and paste form to aid in precise placement and handling of the solder.

Two types of fluxes were used for cell assembly and electrical connections. A rosin flux was used between the solar cell and pretinned copper heat spreader. All other connections were made with a water-soluble inorganic flux that leaves a residue easily washed off with water. The rosin flux residue was removed by special rosin flux removers, or by ultrasonic agitation in acetone.

2.2 PV Module Components

This section describes the individual components in the PV module and their relationship to module performance. An open view of a Type II module is shown in Figure 2.2. The major PV module components are listed below:

- Cell Assemblies
- Fresnel Lens Parquets
- Module Housing
- Module End Cap
- Diodes and Heat Dissipaters
- Electrical Interconnects
- Edge Clips
- Bulkheads and Lens Partition Clips
- Heat Spreader Adhesive
- Dielectric Liner
- External Connectors

The Fresnel lens parquets were positioned directly above the cell assemblies by resting the lens on the housing lip. A set of reference pins on the housing lips that mate to slots in the lens parquet lips ensured precise placement.

The housing served as both the structural support and passive cooling device for the module. The housing was formed from 0.040 inch aluminum. End caps were welded in the ends of the Type I and Type II modules.

Diodes were used for circuit bypass in the event of cell assembly failure. Diodes were mounted on copper stems and heat spreaders for heat dissipation.

Electrical interconnects conducted current between the cell assemblies, and ultimately, to the external connectors. The interconnects were fabricated of copper strips, rather than wire, to reduce electrical resistance losses.

Edge clips, lens partition clips, and bulkheads were used to support the lens parquets and to clamp the lenses to the module. These clips were designed to allow the lens parquet to expand and contract with minimal restraint.

The heat spreader adhesive was used to bond the PV cell assembly to the housing. Both the heat spreader adhesive and dielectric liner functioned as electrical insulation between the active electrical circuit and the metal housing. The heat spreader adhesive also functioned as a thermal conductor between the copper heat spreader and the aluminum housing.

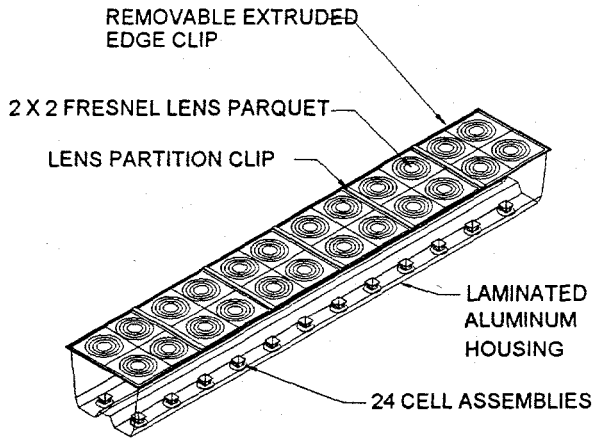

Figure 2.2 "Open" View of Concentrating PV Module

Type I and Type II modules were made during Phase I of this contract. All of the differences between these module types were based on differences in lens parquet size:

Type I module	Type II module
2 x 6 lens parquet	2 x 2 lens parquet
1 lens partition clip	5 lens partition clips
4 bulkhead stiffeners	0 bulkhead stiffeners

The Fresnel lenses were manufactured by American Optical Corporation (AO). The lens was a point-focus type and made of polymethyl methacrylate (acrylic) using injection molding technology. The physical dimensions of the lens were 6.8 x 6.8 inches with a 0.375 inch lip on two adjacent sides. Facets are defined by the material between each tip and valley on the lens. A total of fifteen facets were used in the lens. Twenty-four lenses were required per module. The total lens thickness was approximately 0.250 inch with the facet height approximately 0.125 inch.

Lens parquets were originally designed for a two by six arrangement. This required eight of the twelve lenses to have one of the support lips removed, since lips were molded on two sides. The lens parquet was later changed to a 2 x 2 design due to warpage and anticipated problems in injection molding the parquet as a single piece. Lens warpage was the result of thermal and hygroscopic expansion and contraction. The extent of the errors associated with these problems should be reduced by using the 2 x 2 parquets in Type II modules.

The 2 x 2 parquet was more efficient to produce from single lenses. Lip material did not need to be removed and part handling was less cumbersome. From a manufacturing point of view, the 2 x 2 parquet was practical. As compressive forces on the lens material are a function of part size in compression and injection molding, it is impractical to mold the 2 x 6 parquet as one piece. A 2 x 2 parquet, however, could be molded as one piece.

Single-sided, 0.375-inch wide, 0.005-inch thick, Teflon tape was placed on the lens parquet lip between the lens lip and housing lip. The purpose of this tape was twofold. Primarily, the tape was used to minimize the coefficient of friction between the lens and the aluminum housing. A low coefficient of friction was required to allow the lens to float under the edge clip while being restrained perpendicular to the plane of the lens. The second purpose for the tape was to act as gasket material between the lens and housing.

The module housing was constructed of 0.040-inch thick 5005-H34 sheet aluminum. Aluminum was selected for its excellent thermal characteristics and its superior corrosion resistance. Good thermal characteristics were required since the housing itself acts as the primary cooling system.

The housing was formed into a W-shaped cross section to increase module stiffness and torsional rigidity. Numerical control press brakes capable of 0.5 degree accuracy were used. A 0.4-inch lip was bent at the top of the housing to provide a lens support and clamping surface. The housing shape was designed for a lens-to-cell spacing, the distance from the underside of the lens lip to the top of the solar cell, of approximately 10 inches. The housing design was also appropriate for fabrication techniques such as deep drawing or roll forming. However, initial tooling costs for these techniques were high and impractical for small quantities.

Although housing cross sections were alike for Type I and Type II modules, housing lengths vary. The first modules (Type I) utilized 2 x 6 lens parquets that required only a single partition clip. Later modules (Type II) utilized 2 x 2 lens parquets that required a total of five lens partition clips per module. Each additional lens partition clip added 1.22 inches to the baseline length of the housing. The 1.22 inches included an expansion tolerance for the lenses. The expansion tolerance was determined based on the maximum lens expansion due to thermal growth and hygroscopic expansion. The housing lengths for modules utilizing 2 x 6 and 2 x 2 parquets were 83.84 inches and 88.72 inches, respectively.

The module end caps were used for sealing the ends of the housing and for providing structural stiffness under bending and torsional loading. Type I and II end caps were constructed of 5052-H32 alloy aluminum and were machined to a 0.040 inch thickness.

Several techniques for fabricating the end cap were investigated. Among the most cost-effective were stamping, deep drawing, and casting. All of these methods, however, had high initial tooling costs and were expensive for small quantities.

The end cap was attached to the housing with a continuous weld bead along the edge. Silicone sealant was used on the inside seam to prevent the trapping of water or dust in the cracks. The silicone sealant also electrically isolated the housing from the interior along this seam.

A 0.090-inch right angle bracket was spot welded to the end cap for module to tracker mounting purposes. This bracket extended approximately two inches beyond the end cap on each side. These brackets were installed for testing only per a request from SNL. SKI does not use these brackets for any other purpose. The bottom lip of the end cap was used for a tracker mounting surface.

Schottky rectifiers or diodes functioned as circuit bypass elements in the event of a cell assembly failure. As the cell assemblies were connected in series, a single-cell assembly failure would result in an open circuit for the entire module. Diodes were placed such that a single-cell assembly failure would result in the module current bypassing one-third of the cell assemblies. This was accomplished by connecting one diode in parallel with each series of eight cell

assemblies. A total of three diodes were used for each module. The electrical configuration of the module is shown in Figure 2.3.

The diode was mounted to a copper stand that was solder bonded to a 1.75 inches diameter, 0.062-inch thick heat spreader. The heat spreader design allowed the diode to dissipate the heat generated in the circuit bypass mode.

The electrical interconnects were used for conducting current between the cell assemblies and through the module. The interconnects had a flat strip configuration rather than a wire to reduce resistive losses. The cross-section of the interconnects was 0.016 x 1 inch. The material was 102 OFHC copper. The strips were purchased in 1-inch wide rolls, cut, and formed at SKI.

A stress-relief loop was required in each loop to decrease stresses due to thermal expansion. These stresses resulted from the CTE mismatch between the copper interconnect strips and the aluminum housing. The stress-relief loop was designed to accommodate the expansion mismatch with loads that were less than the shear strength of the top contact solder bond or the cell assembly mounting adhesive. A one-inch tall loop is sufficient strain relief for either the short (6.80 inches) or long (8.02 inches) cell assembly spacing. Stress-relief loops in the interconnects between diodes were also designed to accommodate all of the CTE expansion mismatch with loads that were less that the mount shear strength. The design was modified only to prevent physical interference within the module.

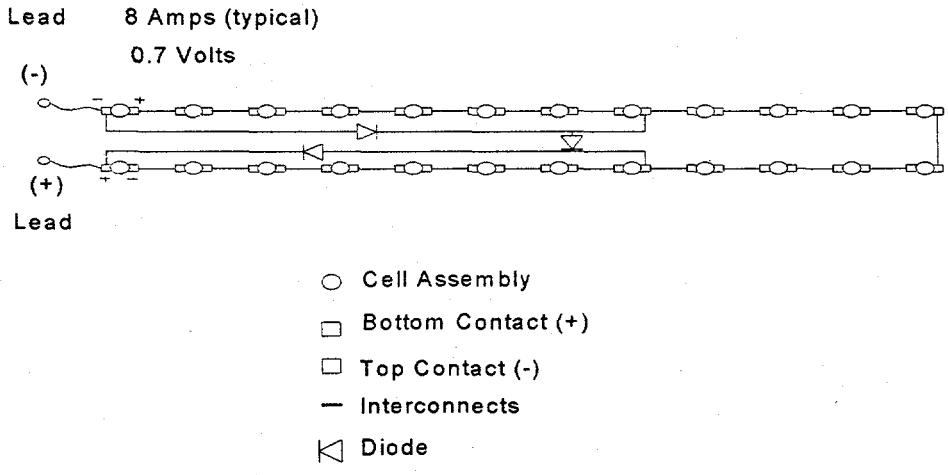

Figure 2.3 Electrical Circuit for the Module

The diode interconnect used the same cross-sectional area as that used in cell assembly interconnect strips. The diode strip width was reduced to allow parallel strips to run on the center stiffener of the module. A cross section measuring 0.5 x 0.032 inch was used with a clearance of approximately 0.5 inch between strips. Strain relief loops were equally spaced to support the strips. Ceramic chips were glued to the housing under the loops to prevent electrical shorting.

The edge clips were used for attaching the lens parquets to the module housing. The clips were designed to apply a linear force of 10 lbs./in. to the lens lip. This was sufficient force to seal the module from rain and dust, but allowed the lens parquet to "float" beneath it. This floating action was necessary to allow the lens parquet to expand and contract due to thermal and hygroscopic effects. A 45° mitered cut was made on the ends to prevent external openings. The clip was fabricated from an aluminum extrusion. The alloy/temper of the aluminum was 6063-T5.

Bulkheads were necessary for structural support in Type I modules (2 x 6 lens parquets), since only a single lens partition clip was used. The Type II modules (2 x 2 lens parquets) used five lens partition clips for sealing and structural support. Hence, bulkheads were not required in the Type II module.

The Type I bulkheads were fabricated from 0.090 inch aluminum, extended the full width of the module, and were approximately two inches tall. A 0.5 inch flange was bent at the bottom of the bulkhead for structural rigidity, and 0.75 inch flanges were bent at the ends for spot welding to the housing.

Four bulkheads were used in each Type I module. No bulkhead was used at the center, because the lens partition clip provided adequate lateral stiffness for the module. The bulkheads were aligned with the parquet bond line and mounted just below the bottom of the lens. This position minimized shading and reduced lens sagging. Bulkheads were used in the Type I module because they were less expensive than lens partition clips.

The lens parquet size was changed from Type I (2 x 6) to Type II (2 x 2) modules to reduce the lens distortion that results from thermal and hygroscopic expansion. The smaller parquet required that four additional lens partition clips be added to the module. The module and lens stiffness requirements were met by the additional partition clips. Consequently, the bulkheads were removed from the module design.

Initially, the lens partition clip was designed as a single piece aluminum extrusion. This design was abandoned because the lens was difficult to insert. The lens was frequently damaged with the single piece clip during assembly.

The edge clip design was modified, and the two piece design simplified lens insertion, and eliminated assembly damage. The clip was also redesigned to reduce potential leak points on the module face.

The spacing between the lens clamping surfaces for the modified clip was designed to match the linear force of the original clip (10 lbs./inch). The depth of the clip was extended to allow screws to be inserted through the side of the module.

The heat spreader adhesive was selected to attach the cell assembly to the module housing and provide a low resistance thermal path between the assembly and housing. Several adhesives were investigated for thermal characteristics, dielectric properties, cure-time, and elasticity. An elastomeric adhesive was used to reduce stresses in the adhesive caused by CTE mismatch between the copper heat spreader and the aluminum housing.

In initial design efforts, the adhesive was also designed to provide the insulation between the housing and cell assembly. The dielectric strength and electrical resistivity of the adhesive bond was subsequently discarded as a design constraint. The insulation between the heat spreader and housing for Type I and II module designs was provided with a laminated film.

A one-part, thermally conductive adhesive manufactured by Shin-Etsu of Tokyo, Japan was used. The adhesive, as purchased, contained 60 percent (by weight) aluminum oxide. Aluminum oxide particle sizes ranged from 0.08 - 0.20 mil (2-5 um). Selection of this adhesive was based on its excellent thermal qualities, and its easily controlled bond thickness due to the small fill particle sizes. The Shin-Etsu adhesive provided a long shelf life, working ease, and exceptionally good thermal properties. The cost of the Shin-Etsu was significantly lower than other adhesives that were investigated with similar properties.

The one-part Shin-Etsu adhesive was a moisture cured adhesive. Moisture-cured adhesives typically take longer to cure than two-part or heat-activated adhesives. No practical method for accelerating was identified. The adhesive cured from the perimeter towards the center. Heat spreaders were removed after three weeks; adhesive near the center of the bond had not fully cured. The diameter of uncured adhesive area was typically 0.5 to 1.0 inches in diameter. Cures were not complete for two to three months. Although the complete cure was slow, the Shinetsu did harden at the perimeter much faster. The module can be removed from the adhesive fixture in approximately three hours.

Heat-activated elastomeric films and two-part elastomeric epoxies were also investigated. Films and elastomeric epoxies were generally more expensive, but did provide shorter mold times. The films also provided better control of adhesive thickness. No complete modules were built with these adhesive systems in Phase I because of time limitations.

The dielectric liner was used to insulate the housing from active electrical components within the module. The potential electrical path identified between the active components and the housing was water entrapment within the module. This water entrapment could occur through condensation or by leaks in the module.

Properties considered in the selection of dielectric liners were dielectric strength, volume resistivity, moisture absorption, UV stability, heat resistance, application ease, and bond strength. Polyesters and acrylics were eliminated early in Phase I. Films and conformal coatings were partially evaluated. Conformal coatings had lower costs and were recognized as the most promising method of preventing internal shorting. Although conformal coat testing continued through Phase I, the application techniques were not resolved.

Typically, films were more costly, but were easier to apply. Several potential dielectric film candidates were commercially available. Several fluorinated and polyvinyl films were considered. The most promising films were Tefzel, Teflon, Tedlar, and Vinyls, all manufactured by DuPont. Tefzel and Teflon films demonstrated excellent properties for dielectric liners. Both films had high dielectric strengths, UV stability, volumetric resistivity, and heat resistance. The resistivity of both film was relatively insensitive to the presence of water.

Tefzel was used as the dielectric liner in Type I and II modules. A chemical etch was used on the film surface to improve the adhesion between the Shin-Etsu and the Tefzel for prototypes. Tefzel was subsequently purchased from the manufacturer with corona etched surfaces, and chemical etching was not necessary. Peel tests indicated the adhesive bond was extremely strong. Tests by SKI for dielectric strength, UV stability, and heat resistance all had favorable results. Cost remained an issue for Tefzel and Teflon. Film costs were not likely to be competitive with conformal coatings that might be fully developed in later project phases.

Several modifications were made to the external electrical power connection design during Phase I. The inexpensive single pin connectors used for both positive and negative leads in previous contracts (3) were discontinued by the manufacturer. A two-pin, 16 AWG connector was identified for use in Phase I. The cost of this connector suggested that custom-made part connector should be investigated in later phases. The two-pin connectors were used in all Phase I modules. The pins were wired together to increase the current carrying capacity with low line losses. Separate connectors were used for the positive and negative lead. A stainless steel grounding bolt was used on prototypes. An aluminum ground lug was used on Type I and II modules to lower costs. External NEMA-rated enclosures with terminal barrier strips were rejected based on preliminary cost analyses. Individual connectors had potentially lower costs.

2.3 Module Objectives And Fabrication

The first generation module design was based on the 300-sun PV concentrator designed by SKI in a previous contract (3). The first generation module, or Type I module, was the baseline SKI module using two each 2 x 6 lens parquets. The second generation module, or Type II module, was the same module using six each 2 x 2 lens parquets.

Module efficiency versus cost was an important factor in the design of a concentrating PV module. A high concentration with an actively cooled solar cell would achieve the highest power output, but not necessarily the highest efficiency. Actively cooled systems resulted in parasitic power losses and had excessively high product costs, as did sophisticated passively cooled systems. SKI chose a simple, passively cooled system to minimize product costs while accepting a small cell efficiency loss due to higher operating temperatures.

2.3.1 Type I and II Module Objectives

The objectives of the first generation module were to evaluate critical mechanical and electrical issues in performance at SNL and SKI test sites. Material evaluation and process development was also based on meeting high volume cost goals.

A mock module with representative lens material was shipped to SNL for environmental testing. Small leaks were apparent during rain tests. Lens distortion occurred during the humidity/freeze cycle tests. During the mock module test cycle, complete Type I modules were fabricated. These complete modules were fabricated for electrical output tests and thermal imaging.

The Type I mock module was tested at SKI after environmental cycling by SNL. The module was pressurized through one of the vent ports, and major leak points were discovered with a leak detection solution. The module housing and lens attachment were redesigned where time permitted in Phase I. Additional improvements were incorporated in later phases of this contract.

Type II module objectives were focused towards eliminating the lens distortion that occurred during humidity freeze cycle tests of the mock module. All of the differences between the two module types were associated with a 2 x 2 lens parquet rather than the 2 x 6 parquet used for the Type I module.

2.3.2 Type I and II Module Fabrication Objectives

Fabrication objectives for Type I and Type II modules were identical. A "design-for-manufacturing" approach was taken in the module design and the fabrication tooling design. Inexpensive tooling, although prototypical, proved the concept of large scale production for the module design. Modules were produced in relatively few steps, and individual steps were amenable to automation processes.

2.3.3 Module Fabrication Tooling

All module tooling was designed for low cost, accurate, fabrication of modules. Cost was the driving factor in this project since virtually all components were in a low volume, development stage. Tolerances were determined by modeling of the module and cell assembly through commercially available software. The budget for acceptable errors were then divided into separate, achievable

budgets for each component placement. The error budgets are listed in Table 2.1. A graph of typical cell efficiency versus placement error is shown in Figure 2.4.

Table 2.1

PV Cell Placement Tolerances

1) Heat Spreader Reference Notches	±.002"
2) Solar Cell Placement on Heat Spreader	±.005"
3) Cell Assembly Placement into Housing	±.020"
4) Installation of Lens Reference Pins	±.010"
5) Lens Dimensional Tolerances	±.010"
Total Error	±.052"
Root Sum Square Error	±.026"

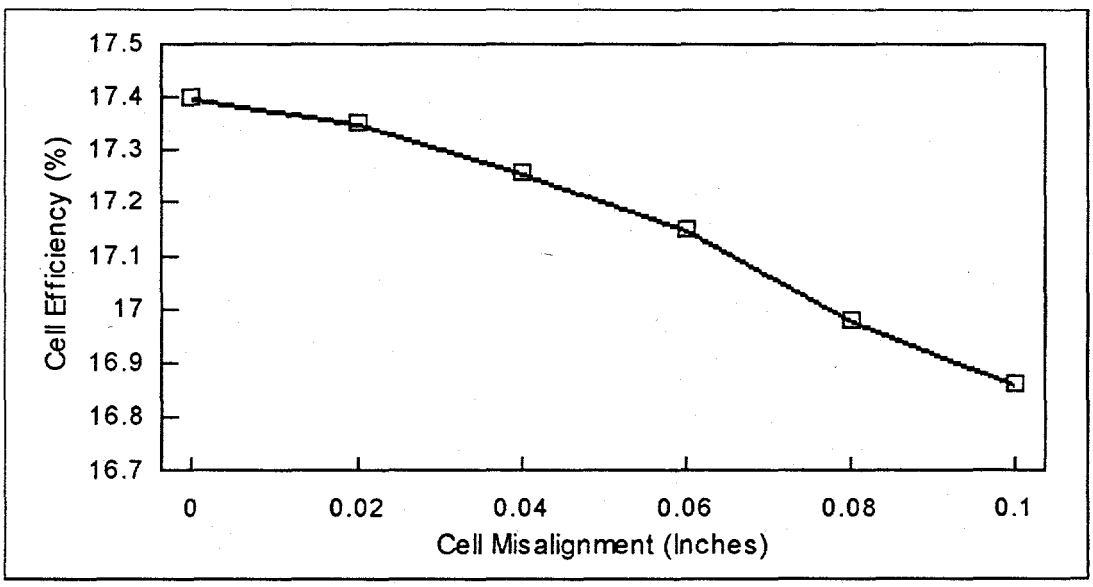

Figure 2.4 Typical Cell Assembly Efficiency vs.Cell Placement Error in Module

2.3.4 Cell Assembly Tooling

The cell assembly tooling went through several design modifications during the course of Phase I. These modifications were necessary due to issues such as solder type modification (paste or sheet), cell assembly component modifications, and potential heat source modifications. After acceptable low-void solder bonds were achieved, emphasis was placed on fabrication efficiency.

Paste solders replaced sheet solders in many locations for ease of application. Fabrication steps that had the highest levels of inefficiency were carefully considered for redesign.

All cell assemblies for modules that were fabricated in Phase I were produced with the initial baseline tooling. The tooling consisted of a 0.25-inch thick aluminum plate used for thermal mass and tooling foundation. A 2.5-inches diameter circle was countersunk for holding the copper heat spreader. Pins of 0.1875 inch diameter were diametrically opposed and placed to fit the location notches punched in the heat spreader. Alignment frames were placed over these pins for precise placement of the solar cell, top contact, and bottom contact. A hollow, Teflon block was used to apply pressure to the top contact fingers during solder reflow. A Teflon peg was inserted in the center of the hollow block to independently apply pressure on the solar cell during solder reflow. A wire clamp was used over the hollow block and peg to apply uniform pressure to the fingers and solar cell. Teflon had the problem of excessive wear after several cell assemblies. A machinable ceramic fabricated by SNL later replaced the Teflon pieces to increase tooling service life.

A temperature-controlled aluminum hot plate was used for the heat source in the cell assembly. The thermal mass of the aluminum plate minimized temperature gradients under the tooling. The temperature was set to approximately 290 °C, and the tooling was placed in contact for 2 minutes and 45 seconds to ensure complete solder reflow. The tooling was then removed from the hot plate, placed on a cooling block, disassembled, and the cell assembly removed.

2.3.5 Cell Assembly Placement Tooling

Cell assembly placement tooling consisted of a series of twelve identical tooling sets for placement of the 24 cell assemblies into the housing. The concept was proven with a single tool set for the placement of two cell assemblies. A tooling set consisted of two sets of tongs with 0.187-inch diameter pins extending from the bottom. The pins were spaced to align with the locating notches on the copper heat spreader and extend approximately 0.050 inch from the bottom of the tongs. The tongs were spaced to place the cell assemblies 6.8 inches apart within the module.

Placement error, parallelism between the tong bottom surface and the housing, and the required force were determined in the initial tooling setup. Spacing tolerance between the two cell assemblies within the tooling was ±0.015 inch. The adhesive thickness under the heat spreader was determined by the distance between the bottom surfaces of the tongs and the module housing.

The tooling accuracy and process control was directly checked by bonding mock cell assemblies to a clear acrylic sheet. Parallelism, flatness, and void ratio were inspected from below the clear sheet.

Tooling sets were bolted to a surface table through pipe spacers with parallel ends. The pipes ensured parallelism and squareness of the tooling with the surface table. The module housing was clamped to the table surface to maintain the squareness while cell assemblies were being glued in place. A pair of precision shafts were used within class "L" fit bushings to maintain accurate placement of the cell assemblies. Negligible lateral movement occurred within the tooling. The shafts were greased to prevent binding or chatter while raising or lowering the tooling.

Double-acting pneumatic cylinders were used to raise and lower the tooling and to apply force during cell assembly adhesive cure. A single cylinder was used for each tooling set. Cylinder pressure was maintained at 25 psi during adhesive cure. A 20 psi cylinder pressure corresponded to a pressure of 2.5 psi on the individual heat spreader. Experimentation indicated that this pressure gave an average adhesive thickness of 0.003 to 0.004 inches.

A regulator and double-acting air control valve were used to divert pressure for raising and lowering the tooling. All inlet ports to the cylinders were plumbed in parallel. The same was done with the outlet (or retracting) ports. The purpose of this plumbing configuration was to raise and lower all tooling sets simultaneously. In use, however, this was not the case. Frictional forces in the cylinders and bushings varied slightly. Minor misalignment in the shafts and bushings also caused varying degrees of static friction. This problem was difficult to correct without joining the tooling sets or setting up an elaborate plumbing configuration. Neither solution seemed economically practical for prototype work, and the problem was accepted. By hand-lowering the tooling sets and using the cylinders for maintaining pressure only, the tooling sets were easily manipulated.

2.3.6 Lens-Parquet Bonding Tooling

The lens-parquet bonding tooling was used for the solvent bonding of the acrylic lenses for the 2 x 2 and 2 x 6 parquets. Tooling consisted of structural beams that clamped the lenses between wooden pads and a granite surface table. The wooden pads and granite table were covered with Mylar sheets to protect the lenses from scratching. The wooden pads were smaller than the lenses to allow access to the bond lines.

A polymethyl methacrylate solvent is used to solvent bond the lenses. The solvent had an extremely low viscosity and was easily drawn into the bond line by capillary attraction. The solvent was dispensed at the bond line with a hypodermic syringe. A slight chamfer was cut into the edge of the lens to act as a track for the needle and prevent spillage to the lens face. Solvent was applied to both sides to ensure a continuous bond line. The lens bond was allowed to cure for a few minutes before flipping the lens parquet for application of solvent to the opposite side bondline.

2.3.7 Cell Assembly Interconnection Tooling

Tooling was fabricated to hold cell assemblies and electrical interconnects in a fixed position during their assembly. The fixture was fabricated from Teflon for high temperature compatibility and thermal resistance. Heat for solder reflow was applied with a 1500 watt soldering iron. A flat tip was machined into the copper tip to expand the effective heating area.

Two sets of tooling were constructed to accommodate the different spacing between cell assemblies. Only two cell assemblies can be put into the tooling at one time. The tooling sets were used alternately in Type II modules as spacing between cell assemblies changes from 6.80 to 8.02 inches.

2.3.8 Reference Pin Locating Tooling

Small studs were pressed into the housing lip and used as reference pins for correct placement and restraint of the lenses. PEM Manufacturing Company supplied the 0.125-inch diameter stainless steel studs. The studs extended approximately 0.080 inch above the surface of the lip. A notch was machined in the lens parquet to mate with the reference pin.

The reference pin locating tooling was used for correct placement of the pins on the module housing lip. A strip of metal with precisely located drill bushings was clamped to the housing lip. Holes were then drilled through the bushings. Pins were press-fit through the holes in the housing lip and lens partition clips. Tolerances on the placement of these holes was ±.010 inch.

2.3.9 Miter Cut Tooling for Edge Clip

It was necessary to construct tooling that would restrain the clips in a desired axis during cutting. A vise set was used to clamp the clip on the outside wall, and a 45° cut was made. Both clips were cut in the same plane. However, fits on the module housing were different for the sides and ends. The sides of the module were sloped at approximately 82° although the ends are perpendicular to the lens. The lower lip of the clip was designed to fit flush with the side wall of the module. The lower point on the clip touched the end cap wall, but did not fit flush. This created a mitered joint in the corners that was easily sealed.

2.3.10 Quality Control Tool for 2 x 2 Lens Parquet

Testing was necessary to qualify lenses prior to installing the lens on the modules. Lens focal length, facet tip and valley losses, and other variables differed slightly from lens to lens. These variables were often a function of lens mold variables that may not remain constant throughout a manufacturing run. For instance, die pressure and material temperature affects facet tip and valley radii during the injection molding process. The die and mold cooling cycle affects cure shrinkage in the polymethyl methacrylate. Cure shrinkage can cause lens distortion thus affecting optimum distance between the lens and cell, and the beam spread.

The lens testing tooling was a square frame mounted approximately ten inches above an adjustable floor. The frame allowed the facets of the lens parquet to extend through while the lens edge rests on the frame. Four cell outlines were scribed directly below the 2 x 2 parquet. The tooling was mounted on a surface table directly underneath a laser. The laser was directed perpendicular to the lens face and was free to move in the X-Y plane. The laser beam was scanned across the lens parquet. Areas with large distortions were easily identified in the refracted beam. The optimum distance between the lens and cell was determined by adjusting the scribe floor up or down. Lens parquets with gross errors or unequal focal lengths were rejected. Typically, this rejection rate was less than five percent.

2.3.11 Module Assembly

The module was assembled in four discrete steps. The first and second step included cell assembly fabrication and module housing fabrication, respectively. These two steps were independent, but occurred in parallel. The third step involved connecting all cell assemblies and diodes, and installation of the cell assemblies in the module. The final step was installation of the SOEs, end caps, lens partition clips, lens parquet, and module edge clips.

2.3.12 Cell Assembly

Surface preparation for soldering of components evolved through the course of Phase I. Initial procedures were time consuming, costly, and inefficient. Early steps for surface preparation included vapor degreasing, acid etching, distilled water rinses, and an alcohol wipe. Eventually, contacts and heat spreaders were vapor degreased at the stamping vendor, and SKI relied only on ultrasonic cleaning in acetone after the assembly of all components.

In the early stages of Phase I, the heat spreader and both bottom and top contacts were pretinned in a solder pot containing 62Sn/36Pb/2Ag solder. Paste solders were substituted for pretinning on the top and bottom contacts for all modules ultimately fabricated in Phase I.

The cell assembly was fabricated by placing all components in the tooling and flowing all solder simultaneously. The pretinned copper heat spreader was set into the tooling, followed by the pretinned cell, top contact, and bottom contact. A tin-lead solder paste was used on the bottom contact and top contact fingers. A tooling clamp applied pressure to the solar cell, and the top and bottom contact.

The cell assemblies were evaluated with several tests. SKI checked all cell assemblies for short circuits with a high potential between the top and bottom contacts. All solder bonds were radiographically examined for voids. SNL performed electrical characterization of the assemblies with a flash tester. The initial solder bond void area was also determined with ultrasonic scans of the

assembly at SNL. All cell assemblies used for modules during Phase I were inspected with these techniques.

Cell assemblies passed all initial evaluation tests prior to being installed in modules. Cell assemblies with similar electrical characteristics (current at maximum power output) were placed in the same module.

2.3.13 Module Housing Assembly

The module housing was fabricated from 0.040 inch thick 5005-H34 aluminum. The aluminum was laminated with 20-inch wide Tefzel film using a pressure sensitive acrylic adhesive. The thickness of the film was 0.0025 inches, and the adhesive was approximately 0.0015 inches thick. A pre-mask film was used over the Tefzel for protection during lamination and metal forming.

Tefzel is a uniaxially oriented film. The film was laminated with the machine direction parallel to the longitudinal axis of the module. The walls and center stiffener of the housing were formed in the laminated aluminum with a numerically controlled press brake. The longitudinal film orientation reduced the stress at the bends. After forming the housing, the film extended approximately 4 inches up the wall on each side for enhanced electrical isolation of the cell string with respect to the module housing in wet conditions.

The availability and cost of the Tefzel films in prototypical quantities presented some problems in early modules. Small quantity samples were received and put into modules as 3 x 3 inch patches underneath each cell assembly. This film was not treated as received, and chemically etching the surface was required for adhesion. DuPont eventually supplied rolls of Tefzel that were corona discharge surface treated by DuPont.

Tefzel film was laminated to aluminum and exposed to ultraviolet (UV) radiation in a QUV Accelerated Weather tester for approximately 2400 hours total. The UV radiation was provided with QUV lamps designated as '340.' These lamps replicated the solar UV spectrum at wavelengths below 350 nm. The cycle was four hours of ultraviolet at 70 °C with uncontrolled humidity (typically 25-50%), followed by four hours at 50 °C in a condensing atmosphere with no ultraviolet. The samples did demonstrate some yellowing in the adhesive layer. There was no apparent change in adhesion.

Following forming, the housing was prepared for welding the end caps. The Tefzel was removed near the end of the housing. This removal was simplified by laminating over a tape mask. An exposed strip approximately 0.7 inches wide was required to avoid weld contamination and prevent film or adhesive failure from heat in the weld area.

Reference pins (PEM studs) were installed on all four sides of the flange at the top of the module housing. These pins were ground to length such that they extended 0.079 inches above the flange. Pins were placed on both sides of

each parquet end. The Type I module (2 x 6 parquet) required six pins; fourteen pins were required for the Type II module (2 x 2 parquet).

Holes were drilled in the housing sides for lens partition clips. Drill bushings and alignment tooling were used to locate holes for precise placement of the clips.

2.3.14 Cell Assembly Connections

Cell assemblies were placed in a template simulating the placement of the cell assemblies within the module. Tooling was slid under pairs of cell assemblies for soldering interconnect strips. Diode heat spreaders and diode strips were soldered into the electrical configuration. Interconnect strips were prepared for soldering by ultrasonic cleaning in acetone. Paste solder was used for all connections.

The entire cell assembly and diode string were transferred to the cell placement tooling. A Teflon mold release agent was applied to the ends of the tooling tongs prior to attaching the cell assemblies. The Teflon film prevented extruded adhesive from adhering to the tooling during placement of the cell assemblies in the module. The tooling was raised and the cell assemblies were placed between the extended tongs. A turnbuckle between the tongs was used to lightly clamp the cell assembly in place.

Approximately 1.0 to 1.5 cc of adhesive was dispensed at the cell location in the housing. The housing was then slid under the cell assembly placement tooling and clamped in place. Alignment blocks provided precise alignment of the housing under the tooling. The tooling was lowered and pressure was applied. Typically, a pressure of 2.5 psi was put on each heat spreader for four hours. After this cure, the individual turnbuckles were loosened, the tooling was raised, and the module removed.

Ceramic wafers were glued into the housing under diode strip strain relief loops. These wafers were used to insulate the strips from the housing, and protect the film from gouging by the copper strips during vibrational loading. The wafers were made of 0.020 inch alumina and laser cut to size. The wafers were also placed under cell assembly interconnects in early modules, but were later deemed unnecessary due to inherent stiffness of the design. The loop-to-housing spacing was typically 0.25 inch.

2.3.15 Final Assembly Steps

The final assembly steps consisted of a series of minor tasks that are postponed until the end of module fabrication. The postponement of these tasks is due to either the fragility of the installed components, or the dependency of installation on completion of prior tasks. For instance, SOEs are installed after cell assembly placement to prevent handling damage during module assembly. End caps and lens partition clips would interfere with cell assembly placement tooling and are necessarily installed near completion of the module.

The SOEs were installed following removal of the module from the cell assembly placement tooling. The SOEs were provided with a pre-mask film to protect the reflective surfaces from damage during forming and handling. The pre-mask was removed after the end caps were welded in place, and immediately before lens installation.

In prototype production, the end caps were welded to the housing after the cell assemblies were glued in place. This order of production was adopted for prototype fabrication only. Cell assembly placement tooling was simplified because the module was slid under the receiver strings, and removed after the assemblies were glued in place. Consequently the placement tooling required only limited vertical travel. In commercial production, the housings will be complete and cell placement tooling will be designed to clear the end caps of the module.

The lens partition clips were subsequently screwed into place, and the lenses were inserted. The lens position was maintained during thermal and hygroscopic expansion cycles with slots machined in the lip of the parquet on all four sides. These slots were machined to precisely fit on the reference pins.

After the lenses were installed in the partition clips, a small, continuous bead of silicone was applied to the underside of the module flange. This bead prevented water from entering the edge clip when the module face is directed downward. The edge clips were installed, and tack welded at each module corner. The small tack welds secured the edge clips during lens expansion and contraction.

The lens parquets were cooled during the tack welding process to prevent lens distortion. A 0.010-inch thick copper sheet was placed under the edge clip at the corners. This copper sheet was actively cooled. The sheet was removed after the lens cooled. Several tests run at SKI resulted in no measurable distortion of the lens under or around the edge clip.

Silicone was injected through a small hole in the edge clips to create the top perimeter lens and module seal. A small bead of silicone was also used on the lens partition and edge clips. The silicone formed a seal around the end of lens partition clip and attachment screws. The junction between the lens partition and edge clip were also sealed with silicone.

2.4 Testing And Evaluation Of Cell Assemblies And Concentrator Modules

This section contains results from tests performed during Phase I activities of the contract. It includes results from tests performed on a set of cell assemblies and analyses of initial samples that did not meet the criteria of the test specifications. With the goal of increasing manufacturability and reliability of the cell assemblies, SKI prepared additional samples for testing. These test results are also included in this document. SNL's evaluation of the electrical performance of a module, fabricated as an activity of this contract, and results of a water spray test conclude this section.

A substantial portion of the text in this section was taken from a report prepared by Marjorie Whipple of the Photovoltaic Evaluation Department of SNL National Laboratories (4). Solar Kinetics would like to acknowledge her efforts and the efforts of others at SNL for their assistance in testing and evaluation of components developed during Phase I of this contract.

2.4.1 Cell Assembly Evaluation

Tests performed under a previous contract, described by Saifee and Hutchison (3), indicated that the solder bond between the cell and heat spreader of the photovoltaic (PV) point-focus cell assembly did not survive all the environmental cycling tests. Thus, this was the first obstacle for SKI to overcome during Phase I of the Concentrator Initiative Contract. In February of 1991, SKI delivered eight cell assemblies for testing according to the specifications outlined in "Qualification of Photovoltaic Concentrator Modules and Cell Assemblies," (2). The following sections describe the results of these tests. Figure 2.5 illustrates the sequence of evaluation tests. The number of lines in the figure correspond to the number of samples that were tested.

The majority of the eight assemblies had at least one top contact finger that slightly overlapped the cell, indicating a misalignment of the top contact on the cell. The top contacts were not identical, and there were burrs attached to some of the fingers. There was flux residue around several fingers. There were no obvious voids between the cell and heat spreader. Cell assemblies made after this batch had production quality top contacts with no burrs on the fingers. Also, these cell assemblies had no misalignment of the top contact.

Cell assemblies were tested with 2200 volts at every connection point within the module. Leakage to ground (the housing) for all modules was less than 0.5 microamps at every point. These hi-pot tests were performed at ambient conditions (approximately 40-80% relative humidity at 27 °C).

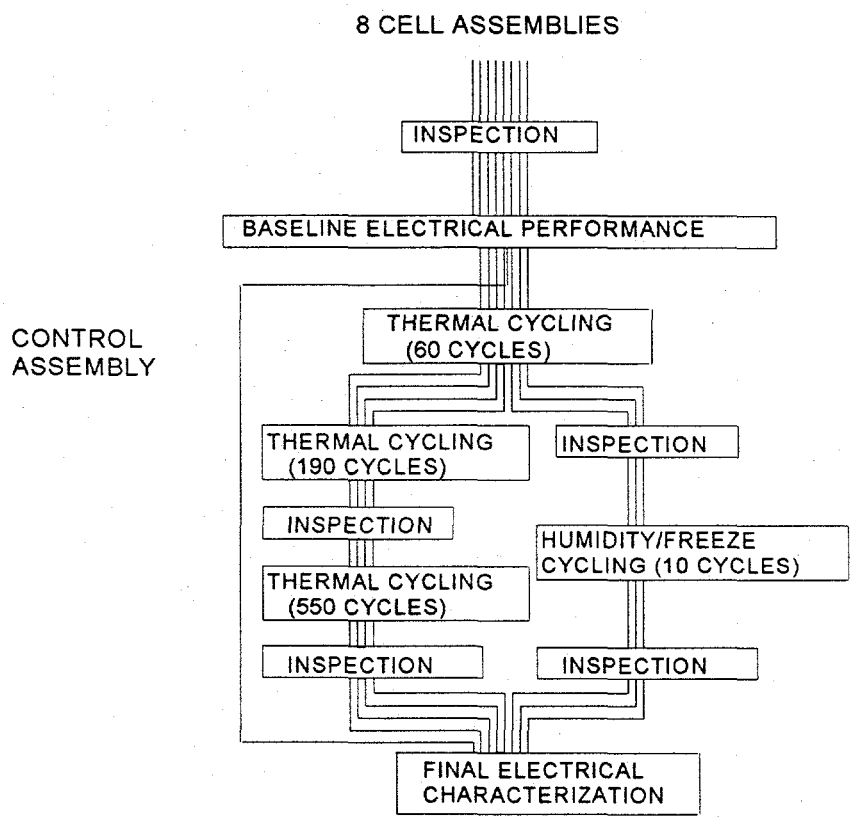

Figure 2.5 Sequence of Evaluation Tests

The number of lines correspond to the number of tested samples

The baseline electrical data for the assemblies are shown in Table 2.2. The performance of the cell assemblies was consistent; each having an efficiency of greater than 19%.

Table 2.2

Baseline Electrical Performance Data

250 X, 25 °C Cell Temperature

Cell Assembly	Isc (A)	Voc (V)	Fill Factor	Efficiency (%)
19-1	8.765	.742	.797	19.45
19-2	8.705	.742	.793	19.22
19-3	8.880	.742	.789	19.22
19-5	9.079	.741	.793	19.68
19-6	9.012	.743	.784	19.27
19-7	8.950	.744	.788	19.79
19-8	8.991	.742	.790	19.53
19-10	8.786	.745	.797	19.41

The ultrasound images used to indicate the quality of the solder bond between the heat spreader and cell were consistent among the eight assemblies. The attenuation was mostly uniform over the cell with the exception of 19-1 and 19-6, where each had small non-uniform areas.

The x-rays showed a dispersion of voided areas. There was no apparent correlation between the non-uniformities in the ultrasound images and light colored areas in the x-rays. The attenuation levels indicated by the ultrasound image for cell assembly 19-6 were lower than the others, and the x-ray indicated many large light colored areas.

X-ray examinations of a material of uniform density will only indicate variations in thickness. Hence, microscopic fractures in the bondline cannot be distinguished. However, small voids were readily apparent. Ultrasound imaging uses the transmittance of the material and can measure large delamination zones with microscopic fractures. The ultrasound image resolution was not adequate to distinguish small voids in the material.

Therefore, to completely quantify the integrity of the solar bond it was necessary to perform both radiographic and ultrasound examinations. This requirement was specific to prototype cell assemblies, and will not be necessary for production volumes.

The cell assemblies were subjected to the temperature shock and humidity/freeze cycles as shown in Table 2.3.

Table 2.3

Summary of Environmental Cycling Tests

Cell Assembly	Shock (Cycles)	Humidity/Freeze (Cycles)
19-1	250	-
19-3	250	-
19-6	250	-
19-7	250	-
19-3	800	-
19-6	800	-
19-7	800	-
19-2	60	10
19-8	60	10
19-10	60	10
19-5	Control	-

Three (19-1, 19-6, and 19-7) of the four cell assemblies exposed to 250 thermal shock cycles suffered an increase in void area between the cell and heat spreader.

The histograms revealed increases in voided area (assumed to be the change in the number of black-colored pixels in the ultrasound images) of the following amounts:

Table 2.4

Change in Void Area After 250 Thermal Cycles

Cell Assembly	Void Area Before (%)	Void Area After (%)	Change In Void Area (%)
19-1	36	52	44
19-3	33	35	6
19-6	39	47	21
19-7	36	47	31
19-5 Control	36	32	-11

Although qualification testing only required 250 thermal cycles, assemblies 19-3, 19-6, and 19-7 were exposed to an additional 550 thermal cycles. The histograms for the corresponding images gave the following results:

Table 2.5

Change in Void Area After 800 Thermal Cycles

Cell Assembly	Void Area Before (%)	Void Area After (%)	Change In Void Area (%)
19-3	33	78	136
19-6	39	81	108
19-7	36	84	133

Table 2.6

Change in Void Area After 250 Thermal Cycles and 10 Humidity/Freeze Cycles

Cell Assembly	Void Area Before (%)	Void Area After (%)	Change In Void Area (%)
19-2	36	43	19
19-8	37	41	11
19-10	36	75	108
19-5 Control	36	32	-11

Inspection of the ultrasound images revealed possible void areas that were not reflected in the count of black pixels shown in the above table. Cell assemblies that exhibit a void area increase of more than 10% do not pass this test; therefore, these cell assemblies did not pass the environmental cycling tests.

Cell assemblies 19-1, 19-2, 19-5 and 19-8 were cross-sectioned and photographed to determine the cause of failure. The layers of interest are shown in Table 2.7.

Table 2.7

Cell Assembly Component Materials and Thicknesses

Material	Approximate Component Thickness (um)
Silicon Cell	200
Aluminum	500
Titanium	120
Palladium	50
Silver	9
Lead/Silver Solder	25
Copper Heat Spreader	1590

Material scientists at SNL inspected cell assembly 19-10. This cell assembly separated at the cell/heat spreader interface during post-cycling inspections. Using a scanning electron microscope, SNL detected aluminum oxide on both the cell and the heat spreader of cell assembly 19-10. Details of the analysis are included in Appendix D of the Phase 1 report (1).

In order to determine the cause of the delamination, five electrically inactive cell assemblies were subjected to 10 humidity/freeze cycles as described in reference (2) without any humidity control. That is, the relative humidity in the environmental chamber was constant and approximately 50% throughout the test. There was no change detected in the images; therefore, the humidity caused the failures in the previous set of cell assemblies. In conclusion, cell assemblies that were humidity/freeze cycled failed by delamination of the aluminum layer from the solar cell. Cell assemblies subjected to thermal shock cycling had increases in void areas that did not meet the test acceptance criterion.

The cell manufacturer was contacted and was aware of the fact that the cells fail under high temperature, high humidity environments. The cells were tested by the manufacturer for 30 days at 95% relative humidity (non condensing) and 45 °C, a less severe qualification test than that specified by Reference (2).

All cell assemblies were electrically characterized after completing the environmental cycling tests. A summary of the electrical data is shown in Table 2.8.

Table 2.8

Final Electrical Performance Data and

Efficiency Loss After Environmental Cycling

250X, 25 °C Cell Temperature

Cell Assembly	Isc (A)	Voc (V)	Fill Factor	Efficiency (%)	Efficiency Change (%)
19-1	8.524	.743	.790	19.03	-2.2t
19-2	8.604	.744	.646	15.65	-18.6h
19-3	8.638	.742	.786	18.99	-1.2t
19-5	8.856	.740	.789	19.44	-1.2c
19-6	8.694	.741	.782	18.97	-1.6t
19-7	8.688	.744	.785	19.05	-3.7t
19-8	8.609	.744	.665	16.07	-17.7h
19-10	0.686	.700	.325	7.14	-63.2h

c Control Unit
h Subjected to Humidity/Freeze Cycling
t Subjected to Thermal Cycling

The cell in 19-10 separated from the heat spreader during handling. Therefore, the electrical data for this assembly were not reliable. As shown in Table 2.8, the assemblies exposed to thermal shock demonstrated acceptable electrical performance.

The cell assemblies did not survive the qualification tests outlined in Reference (2). Cell metallization layers failed during the humidity/freeze cycle; unacceptable increases in void area occurred during thermal shock cycling.

2.4.2 Soldering Studies

Several alternate soldering techniques were attempted to increase the reliability and reduce the cell assembly manufacturing costs. SKI performed experiments using an alternate material for cleaning the components prior to soldering cell assemblies. Solder paste was also substituted for foils. SKI tested cells made by Spectrolab in place of the ASEC cells that had been used in the past. Details of these studies are included in this section.

SKI attempted to use a new, nontoxic material for cleaning the cell and heat spreader. Out of five cell assemblies, only cell assembly 22-38 had a large unbonded area between the cell and the heat spreader. More evaluation is needed to verify the adequacy of this cleaning material.

SKI engineers used a paste solder for the cell-to-heat spreader bond. This method had potential manufacturing cost savings and could increase the yield by producing more consistent solder bonds. Ultrasound tests indicated that this technique produced unreliable bonds after 250 thermal shock cycles. Inspection of the cross sections of cell assemblies 30-10 and 30-7 revealed that out of ten cell assemblies, the solder bond itself cracked during cycling. Two other assemblies, 30-6 and 30-11, delaminated after 500 thermal cycles. Failure occurred because of the large number of small voids in the bond. These voids probably formed as paste binders outgassed during soldering. The solder layer also appeared to be much too thin to withstand the stress induced during thermal cycling.

SKI manufactured five cell assemblies using Spectrolab cells. The cell-to-heat spreader solder bonds did not withstand thermal cycling tests. One cell assembly was stored as a control unit, and the other four were subjected to thermal shock cycling. Significant increases in void areas are evident in cell assemblies 31-2 and 31-5 after 250 thermal cycles. Four samples were subjected to a total of 500 cycles because SNL was considering more severe test specifications than were used for Phase I. Table 2.9 summarizes the estimated change in void area from the initial scan as determined by the number of black pixels on the ultrasound images.

Table 2.9

Estimated Void Area of Cell Assemblies

With Spectrolab Cells

(All values are changes in void area from initial scan)

Cell Assembly	Baseline	After 250 Cycels (%)	After 500 Cycles (%)
31-1	42	7	88
31-2	40	43	103
31-3 Control	40	-	-
31-4	38	14	95
31-5	38	26	74

Cell assembly 31-1 was the only sample that exhibited a void area increase of less than 10% after 250 cycles. In order to inspect the bond between the cell and the heat spreader, SKI destroyed cell assembly 31-1 for inspection after it

had been subjected to 500 cycles. It appeared that a water-based flux was causing voiding in the bond. Thus, the use of a rosin-based flux was suggested.

2.4.3 Module Evaluation

Two Type-I modules were fabricated during Phase I of this contract. Both were populated with cell assemblies that were electrically tested in the Photovoltaic Device Measurement Laboratory (PDML). One module was sent to SNL for electrical characterization and water spray evaluation. The results of these tests are included here. SKI also built two Type-II modules that were evaluated during Phase II.

2.4.3.1 Cell Assembly Performance

The 24 cell assemblies included in module PV-SKI-Type I-2-0991 were selected from a group of 35 assemblies that were previously tested at SNL. The assemblies were ultrasonically scanned for possible voids by the Non-destructive Testing Technology Division and electrically tested in the PDML. The 24 cell assemblies with the largest current at the estimated maximum power point, I_{mp}, were selected for use in the module. The I_{mp} at 240 suns concentration ranged from 6.8 to 7.5 Amps. The average voltage at the maximum power point, V_{mp}, for the 24 cell assemblies was 0.61 Volts. The average efficiency of the 24 assemblies was 17.2% at reference conditions of 1000 W/m^2 and 25 °C cell temperature.

2.4.3.2 Module Performance

The module was mounted on the Motorola tracker at the Photovoltaic Technology Evaluation Laboratory (PTEL), and I-V curves and associated weather data were recorded at regular intervals for several hours. Typical current versus voltage and power versus voltage curves are shown in Figure 2.6. Note the "step" in the curve where the voltage is approximately 8 Volts. Shading tests indicated that this step was caused by the last one third of the string. Since this string produced the least amount of current, the bypass diode was forced to leak some of the module's current. This clearly illustrated the need for matching the 24 cell assemblies for current at maximum power within a module.

When processing the performance data, SNL discarded I-V curves that were recorded when the ratio of the Isc to DNI (corrected to 1000 W/m^2) dropped below 6.82 Amps because of the possibility of tracking errors or spectral changes. They also eliminated data taken when the azimuthal tracking error was greater than 0.5 degree from normal and data which revealed a V_{mp}/V_{oc} ratio of less than 0.79.

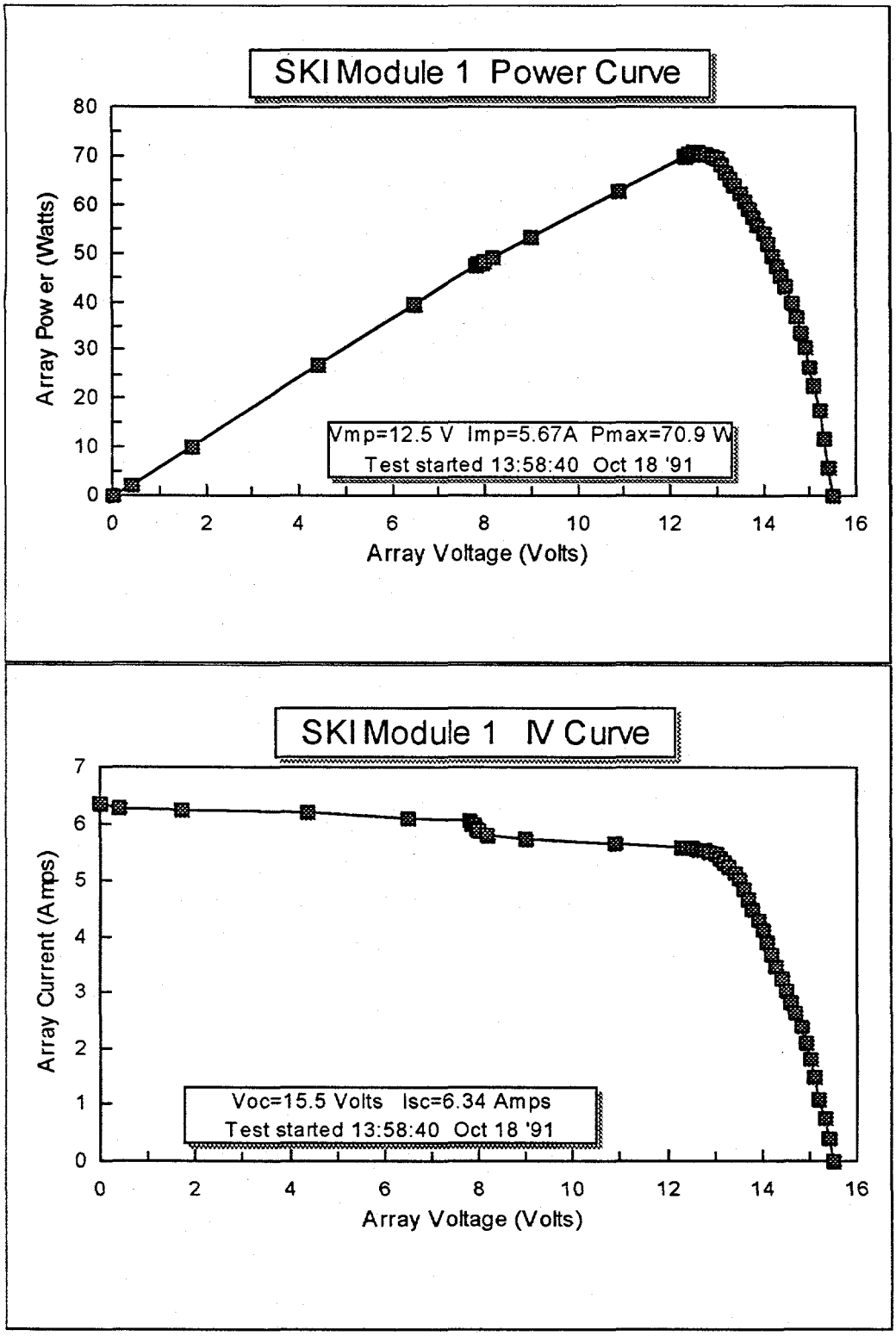

Figure 2.6 Typical Type I Module I-V and P-V Curve at Operating Conditions

Figure 2.7 shows the results of the October 18th test. A regression fit of that data resulted in the following formula for calculating Pmax at 65 °C < T_C < 80 °C and 850 W/m^2 < DNI < 940 W/m^2:

(1a) Pmax = -0.284 T_C + 0.0670 DNI + 31.5

where:

Pmax is the maximum power output, W

T_C is the cell temperature, °C

DNI is the direct normal incidence, W/m^2

The 95% confidence limit is 3 x 0.208, or 0.6W.

Also, module efficiency (Eff.) can be calculated using the following formula:

(1b) Eff. = -0.0389 T_C - 0.00171 DNI + 14.3

The 95% confidence limit is 3 x 0.0286, or 0.09%.

Figure 2.8 shows the results of the October 21st test. Regression fits for this second set of data yielded the formulas (2a) and (2b) for maximum power and module efficiency at test conditions of:

50 °C < T_C < 60 °C and 700 W/m^2 < DNI < 850 W/m^2:

(2a) Pmax = -0.200 T_C + 0.0826 DNI + 12.4

The 95% confidence limit is 3 x 0.186, or 0.6 W.

(2b) Eff. = -0.0303 T_C - 0.0004 DNI + 12.5

The 95% confidence limit is 3 x 0.0299, or 0.09%.

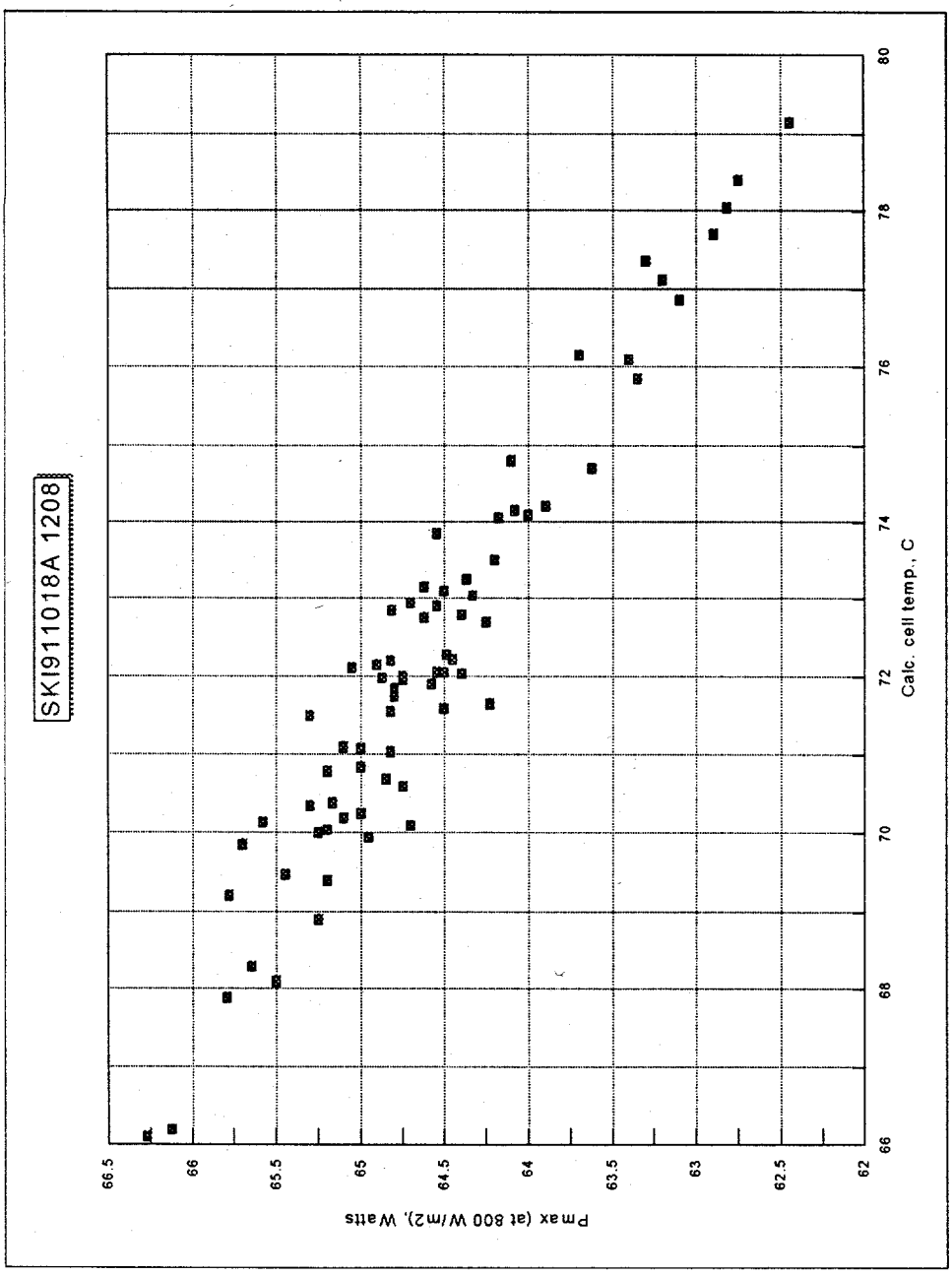

Figure 2.7 Power Produced by SKI Module on October 18, 1991

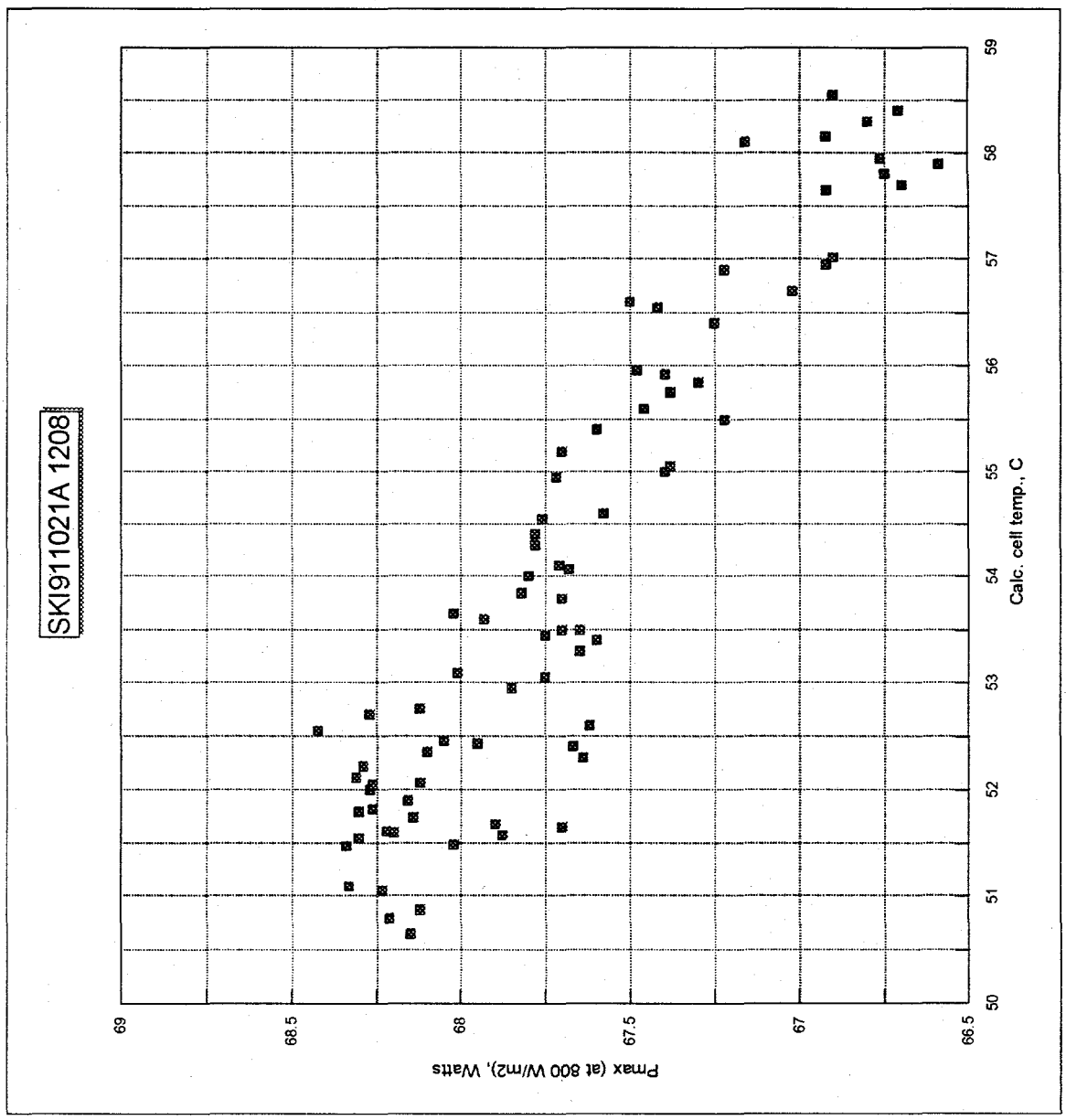

Figure 2.8 Power Produced by SKI Module on October 21, 1991

Using these equations, the power output of the module at 850 W/m^2, DNI, and 70 °C, calculated cell temperature, was 69 ± .6 Watts. The efficiency under these conditions, based on the module total area, was 10.1 ± .09%. This efficiency approached the theoretical limit achievable with the module geometry, solar cells, and lenses used. Additional losses are within the measurement errors and considered insignificant.

2.4.3.3 Water Spray Test

The module was subjected to a water spray test. After 1 hour of exposure to spray, the module had accumulated 1.5 liters of water. SNL noticed beads of water on the module walls, indicating that water leaked around the edges of the lenses. There were no particular locations that leaked more than others; that is, water leaked from various locations around the perimeter.

2.5 Tracker Design And Fabrication

The initial approach to the tracker prototype design was a 1 kW array based upon a polar drive configuration. After reviewing the conceptual design, it became apparent that the geometric constraints inherent with the polar drive approach would make a 20 kW array awkward and impractical. Therefore, all of the preliminary design effort was suspended and alternate tracker formats were studied.

The chosen alternate to the polar drive was an azimuth/elevation (Az/El) drive design. This alternate layout could easily scale to the higher power requirement and eliminated the required sun sensor development work for the polar tracker. The following sections give an account of the preliminary polar drive design and the subsequent Az/El drive design and construction.

2.5.1 Polar Drive

The major advantage of a polar configuration was the simplicity of the tracking control. With proper alignment of a polar (hour) axis, tracking is limited to a continuous hour angle update about the polar and daily updates about the declination axis. The baseline design developed by SKI used a passive sun sensor for closed looped tracking about the hour axis and a combination open/closed loop "hybrid" configuration for the declination axis daily update.

The disadvantage of the polar drive system was the complexity of the array structure (Figure 2.9). For small power configurations, the physical complexities were offset by the simple tracking requirements. However, when these polar systems need to accommodate photovoltaic array's in the 20 kW range, the array structure became ungainly. SKI's attempts at scaling up the 1 kW array to the 20 kW array revealed that the top of the hour axis would reach a height of 60 feet when located at a latitude of 50 degrees. Therefore, the preliminary polar drive design was suspended and alternate tracking configurations researched.

2.5.2 Azimuth/Elevation Tracker

The inherent restrictions of a polar drive geometry limited the number of modules that could be mounted on a single tracking platform. The physical characteristics of an Az/El tracker gave it the capability to scale to the larger array configurations. The 2 kW prototype tracker array developed by SKI in Phase I can be easily scaled to the required 20 kW array. This prototype design of this platform included the concentrating module support frames, Az/El drive stage, and the array support pylon (Figure 2.10). The design provided for ease of assembly, efficient knock-down and shipping, and the capability to operate at all latitudes.

The Az/El support system required simultaneous tracking in two axes. Dual axis shadow band tracking was rejected because of potential problems when the sun's image is lost. With a polar drive, the sun could be reacquired by driving the array east/west about a single axis. Sun reacquisition with Az/El trackers was complicated by requirements to update two axes by different and unknown amounts.

A microprocessor was added to the tracker platform to resolve the problems with continuous updates for two axes. Microprocessors capable of supplying information for tracker updates during reacquisition were easily programmed for an open loop tracking system with no shadow band trackers. The Phase I tracking design was redirected to an open loop system when the Az/El geometry was established.

SKI developed load cases for structural design, with deflection limits based on tracking accuracy. The load cases used for design were:

1. Track in all array orientations with a combined wind load (steady state and gust) of 27 mph with no structural deflections totaling more than 2 milliradians (mrad),
2. Drive to stow (array parallel to ground, lenses face up) from any orientation with a wind load of 50 mph without exceeding stresses allowed by the American Institute of Steel Construction (AISC) code,
3. Survive without permanent damage while stowed in combined winds of 90 mph and not exceed stresses allowed by the AISC code (5).

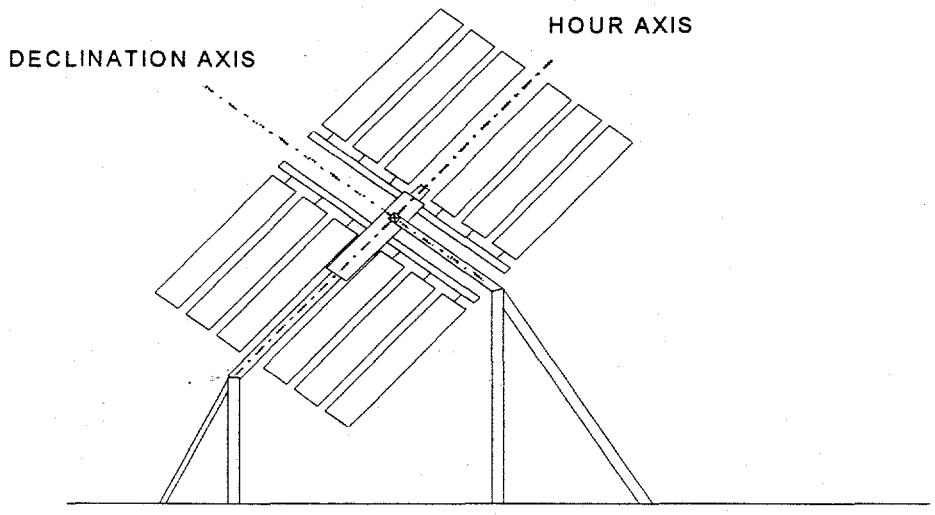

Figure 2.9 Schematic of 1 kW Polar Tracking Concept

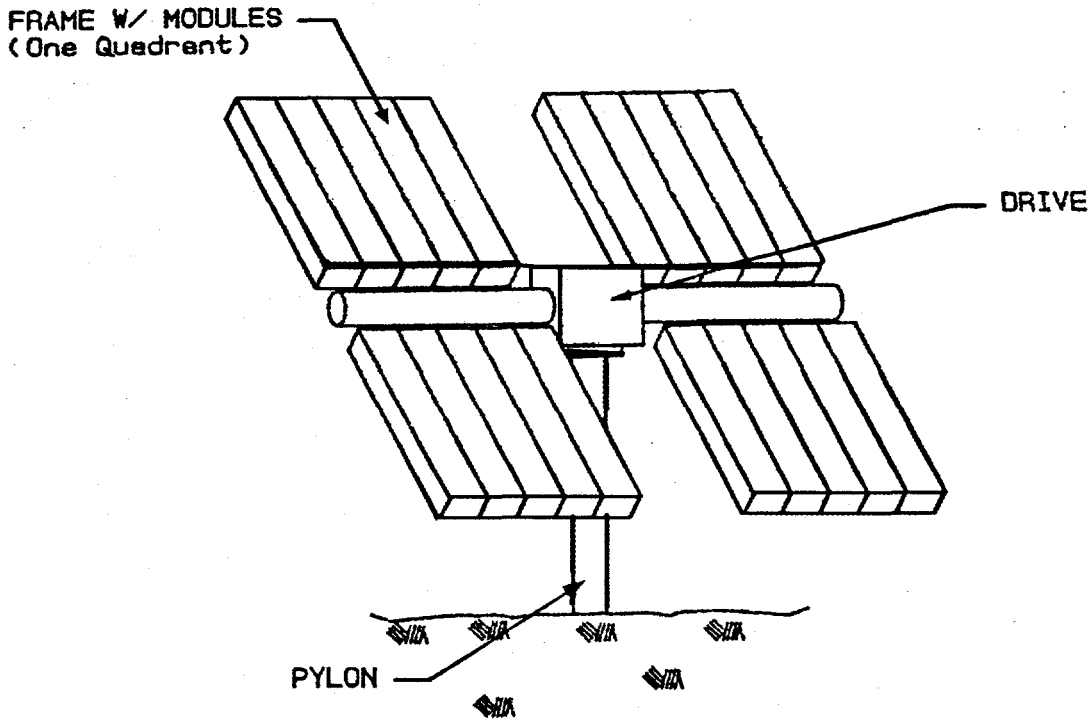

Figure 2.10 Schematic of 2 kW Az/El Prototype Tracker.

These guidelines required that the combined structural deflections of the frame, drive, and pylon under operating conditions remain less than 2 mrad. The budget was arbitrarily divided between the drive and pylon (1 mrad each).

In addition to structural deflections, 2 mrad of error was allowed for tracking controls. An error of 1 mrad was allowed for miscellaneous effects not identified in Phase I. Consequently, a total tracking error of approximately 5 mrad was defined as the goal for the 2 kW tracker.

This error budget was based on keeping cell efficiency losses small. Computer simulations of the SKI concentrating PV module's relative power output as a function of tracking error were developed from software written by Larry James. The results are summarized in Figure 2.11. The solar cell output drops 1.3% when the module is approximately 5 mrad off axis.

2.5.2.1 Azimuth/Elevation Drive Design

Finite element analysis was used to establish stress and deflection in the module frame; the Az/El drive stage was analyzed using handbook equations; and the support pylon analysis was performed from a spreadsheet developed at SKI.

Wind load values were derived from the coefficients established by J.A. Peterka (Phase One; Individual Array Tests, reference 6). The loads at the array pivot center were used to analyze the module frames. Analysis of the drive stage and support pylon used the loads present at the pylon top.

2.5.2.2 Module Support Frames

The module support frame combined four identical array quadrants with central torque tubes (Figure 2.12). Each quadrant was composed of two frame spars, two cross bars, and two tie rods. The frame spars were fabricated from (M6 x 4.4) ASTM A36 I-beams. The cross bars were made from 2 x 2 x 1/8 ASTM A36 angle. Low carbon bar was used for the tie rods. The torque tubes, which provided both the central spine of the array and the elevation axis, were made from ASTM A519 8.625 inch O.D. mechanical tubing. All components were readily available structural steel shapes.

Array design was based on the support of 20 modules (five modules per frame). A three point connection between the array support and concentrating module was chosen to eliminate twist from attachment. A friction connection was designed to accommodate the thermal expansions and the mechanical deflections of the module.

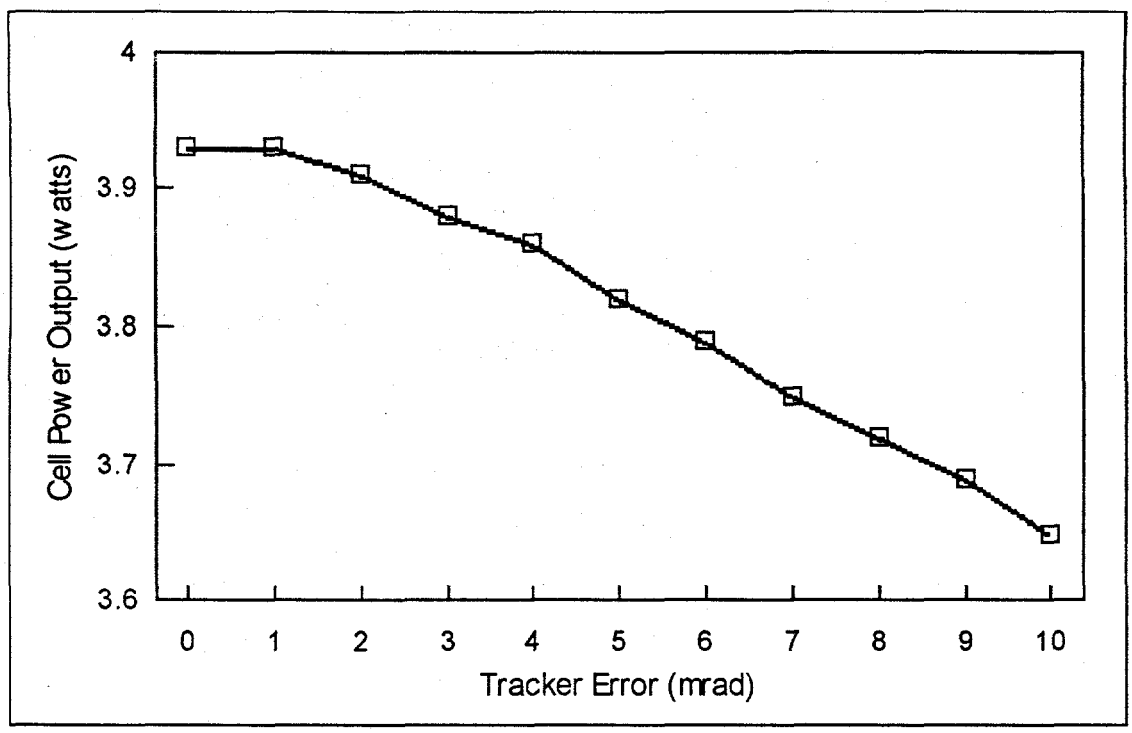

Figure 2.11 Cell Assembly Electrical Output vs. Tracking Error

2.5.2.3 Module Frame Static Analysis

The finite element analysis (FEA) code used to determine the frame stress and deflections for each load cases was the Integrated Design Software Package from The Engineering Software Company. The structure was modeled as a three dimensional (3-D) space frame. Symmetry of the 2 kW array was used to decrease computer time. The model consisted of two module frames fixed to one torque tube. The drive connection was modeled as a fixed support.

The array orientation for each wind load case that produced the most severe force and moment load coefficients from reference (6) was selected. Zero degrees azimuth corresponded with a wind direction that was perpendicular to the array face. The elevation angle was zero degrees when the modules were perpendicular with the ground. For the 27 mph and 50 mph conditions, the worst case position was at an azimuth and elevation angle of zero degrees. The 90 mph case was oriented with a zero degree azimuth angle, but the elevation angle was 90 degrees (stowed position).

The wind loads, frame weight, and module weight were applied to the finite element model in accordance with the array's orientation. The combined wind loads were divided by the total number of modules present on the 2 kW array (20) and applied at the module support points. The frame weights were dependent on the design iteration. The 32 lbs for module weight was constant throughout the analysis.

The wind loads for case three (90 mph, stowed position) were much lower than those of case one (27 mph) and case two (50 mph). Therefore, case three was not analyzed.

The FEA static analysis results for case one and case two are shown in Table 2.10. The maximum root sum squared (RSS) deflection of the module support frames was 0.590 mrad at 27 mph. The maximum stress in the frame at 50 mph was well within the requirements of the AISC code (5).

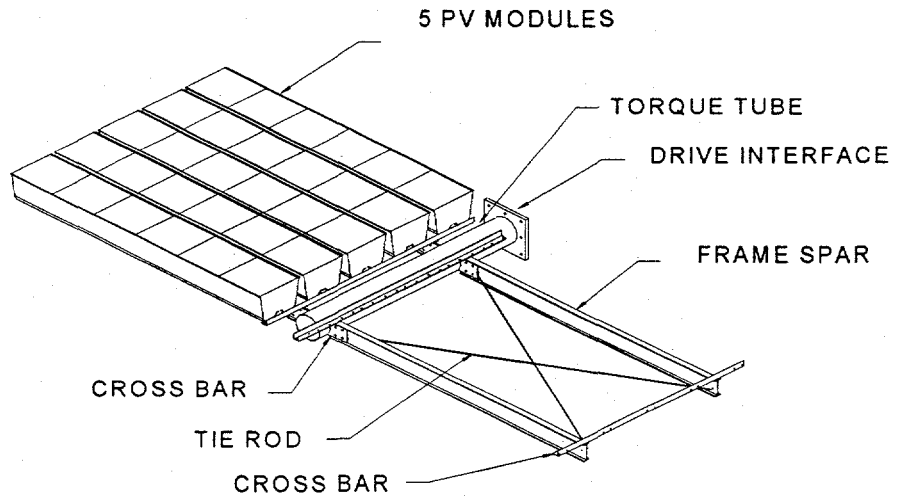

Figure 2.12 Tracker Frame Assembly

Table 2.10

Finite Element Analysis For Static Loads

Case One: 27 MPH, AZ = 0°, EL = 0°

Axis	Deflection (mrad)
Elevation	0.46
Azimuth	0.37
Total RSS Error	0.59

Case Two : 50 MPH, AZ = 0°, EL = 0°

Frame Component	Stress (psi)	Safety Factor (Beyond AISC Code)
Torque Tube	7240.0	4.97
Frame Spar	5390.0	6.68
Cross Angle	4233.0	8.50

SKI chose to use commercial hot rolled structural shapes on the tracking platform to keep material costs low. The error increased beyond the budgeted value when the next smaller structural shape was selected for components. Stresses were considerably less than those allowed by the AISC code. Clearly, the frame design was governed by the deflection restriction of 1 mrad at 27 mph.

2.5.3 Azimuth/Elevation Drive

The primary emphasis in the drive design was cost effectiveness. Early commercial markets will probably support only low and medium production volumes. Consequently, intensive manufacturing methods such as casting, long-line boring, large-vertical turning were avoided. Large diameter ball bearings that require custom manufacturing and extensive seat machining were also avoided. Wherever practical, commercially available power train components were selected.

The drive was intended to serve as both a test platform for module development as well as a first production prototype. As such, low risk was also emphasized to ensure reasonable design and a rapid development effort. Highly stressed parts were avoided to keep component testing at a minimum. The drive selected for Phase I was conservatively designed. Hence, future production drives could be simplified and lightened for lower manufactured costs.

Finally, the drive was designed to be readily serviceable. The design concept, selection of components, and specific design geometry all contributed to achieving a design that allowed easy repair and maintenance.

The main body of the drive was a flat steel plate. The sides of the plate cradled the center section of the elevation axis torque tube. The torque tube center section was simply a tube with two square flanges, one either end. The outer torque tube sections, which each carry half of the array, had matching flanges.

The support pylon had a flat flange at its top with a stub of shaft extending straight up from its center. The drive base plate sets on that flange. The stub shaft protruded through the base plate and engaged the azimuth drive gear reducer. A lower pressure plate under the pylon top flange bolted to the drive base. This captured the pylon top flange and secured the drive to the pylon. Bearing material between the flange, pressure plate, and drive base plate permitted relative motion.

2.5.3.1 Elevation Drive

A jackscrew drive was selected for the elevation axis because that approach had been well proven over many years on a wide variety of solar collectors. Commercial jackscrews were available with very low or no backlash. Jackscrews were also available in a wide range of load ratings covering the entire spectrum of anticipated loads from the 2 kW through the 20 kW array.

Sectional synthetic bearings were used to simplify the elevation axis bearing support. Roller bearings were not considered because of the cost associated with the bearing and the machining required to support and mount them to a shaft. The synthetic bearings were arranged as two pairs of self-aligning V-block supports. They bore directly on the center section of the elevation torque tube. The self-aligning feature reduced the required accuracy of manufacturing, which reduced costs. Two restraining straps lined with the same bearing material were clamped over the tube section to create a simple zero play assembly. These straps were also self-adjusting to accommodate the wear anticipated in the bearings. The fluorinated bearing material was specifically compounded for low speed, non-lubricated sliding applications against carbon steel. The commercially available material was well demonstrated in such applications as gib ways on large machining centers and turret bearings on military vehicles.

2.5.3.2 Azimuth Drive

The azimuth drive required more than 360 degrees total travel in order for the array to be functional at any latitude. This requirement eliminated the option of using a simple jackscrew drive for azimuth motion. A gearbox was the most straightforward method of providing the range of travel, high torque, and slow motion required for the azimuth rotation. A standard commercial gear reducer

was selected for this task although this led to the necessity of a drag brake for backlash control.

The azimuth stage was built on a single-steel base plate. The simple design permitted almost all parts to be flame cut without additional machining. Little post-machining was required after welding.

The standard gear reducer was face mounted to the top of the base plate where it rotates with the azimuth stage. Horizontal wind drag loads were reacted through the gearbox bearings to the support pylon. Overturning and vertical loads were reacted to the pylon through plain synthetic bearings between the bottom of the base plate and a flange at the top of the pylon. As with the elevation bearing support, the synthetic bearing in the azimuth drive permitted loose tolerance fabrication in a zero play assembly. The synthetic bearing material also provided long life with zero lubrication and was adjustable to compensate for wear.

2.5.3.3 Backlash Control Drag Brake

Backlash is the relative motion between input and output shafts, when the input shaft is locked. The motion typically occurs because of the cumulative clearance between meshed gear teeth of each reducer stage. Backlash is a problem in precision drives if a load reversal, such as a change in wind direction, occurs. Precision commercial gear boxes with low backlash were available, but expensive. A drag brake, combined with a standard gear reducer, was selected for the Phase I tracker to reduce cost.

The drag brakes for the 2 kW tracker effectively eliminated backlash by applying a constant braking action to the driven shaft. For the PV array drive, the braking torque applied was equal to the wind induced azimuth torque for a 27 mph wind at the worst array orientation. The gear set was always loaded in one direction. Consequently, the drag brake eliminated problems with backlash because it prevented load reversals.

Parasitic power consumption of the array drive was increased because the motor must always overcome the drag brake friction force as well as wind and weight loads. For the PV array drive, the total cumulative time of motion per day was very low. Also, the speed of rotation was very low. The combined effect of slow speed and infrequent motion was a negligible brake parasitic power consumption, estimated to be 0.15 kW hr/day.

Slip-stick motion is a phenomenon that occurs in drag brake drives because most material combinations have differing static and dynamic coefficients of friction. Starting from rest, the input torque is gradually increased until the brake begins to slip; that is the static brake friction is exceeded. At this time, there is relative motion between the brake and rotor so the dynamic coefficient governs the friction; and therefore, the torque developed. When the dynamic coefficient is less than the static, the brake force is reduced as motion begins and the output shaft accelerates. Slip-stick is a problem in tracking drives because the

load needs to be moved slightly, and the sudden acceleration can cause overshoot, and thus, positioning error.

The brake lining material selected for the 2 kW tracker was a fluorinated plastic and was also used as the material for the synthetic bearings. It was selected because of the exceptionally low difference between static and dynamic friction coefficients. Consequently, the slip-stick motion that can occur with drag brakes was not a problem for the tracker. The material also has very low wear properties when run against steel.

2.5.3.4 Design for Serviceability

Minimizing total life cycle cost was a goal of the current design. To do this, the unit must be reliable and easily maintained. Numerous design features were included in the PV array drive to reduce maintenance needs and maintenance costs.

Wherever possible, key components were replaceable or repairable without removal of the array from the support pylon. This was a departure from many existing solar array drives designs. The following components may be removed without disturbing the array:

- Azimuth gear reducer,
- Elevation jackscrew actuator,
- Elevation axis bearings,
- Azimuth overturning and vertical bearings,
- Azimuth anti-backlash break pads,
- Azimuth drive motor,
- Elevation drive motor,
- Azimuth axis encoder, and
- Elevation axis encoder.

The drive was designed such that no specialized equipment was required for removing these items. The synthetic bearings can be relined and replaced with very simple tools. The gear box and encoders were designed to be replaced, with repair performed by a factory agent. The jackscrew was essentially a disposable unit because of its low cost. The gearbox was manufactured by a company with worldwide stocking distributors and assembly operations. The jackscrew was manufactured by one of the world's largest manufacturers of linear actuators.

2.5.4 Support Pylon

The support pylon was a mechanical tube with a 9-inch O.D. and a wall thickness of 0.25 inch. Its mechanical properties met all of the requirements of ASTM A519. The pylon had a bolted flanged connection at the azimuth drive stage for ease of assembly and positioning. The pylon extended ten feet below grade. The tube was perforated with staggered 6-inch diameter holes below grade to allow for concrete fill.

A spreadsheet was developed in Phase I to perform pylon design iterations. Eight parameters were variable, and the response to bending and torsion loads, as well as column loading, were reported in a final design summary. The inputs for each computation were:

1. wind speed,
2. array orientation,
3. pylon physical dimensions,
4. pylon material properties,
5. overall array dimensions,
6. array weight, and
7. wind loads.

The results from combined bending and torsion were reported as Von Mises stresses, the direct shear stress from lateral loads, the angular deflections of the pylon top, and the angular twist of the pylon. For column loading, a design figure of merit was reported along with a flag to indicate that the pylon was susceptible to local buckling.

The effects of bending and torsion were based on the handbook calculations of Roark for Beams under Simultaneous Axial and Transverse Loadings (7). The normal stresses predicted by Roark were combined with torsional stresses in the manner of Von Mises to give the maximum effective stress in the pylon (8). Acceptable column loading was determined with the interaction method as illustrated by Beer and Johnston and in accordance with Section 1.9 of the AISC code (9,5).

These results are reported for the final design iteration in Table 2.11. The three wind design cases (see section 2.5.2.3.) produced stresses substantially below those allowed in Section 1.5 of the AISC code (5). The pylon design was governed by deflection under operating conditions.

The total root sum square (RSS) deflection of the pylon at 27 mph was calculated to be 1.46 mrad. This value exceeded the initial 1 mrad deflection budget for the pylon. However, when summed with the zero backlash of the drive and the 0.59 mrad deflection of the frame the total structural deflection was equal to 2.05 mrad. The total deflection exceeded the targeted 2 mrad deflection budget for the tracker by only 2.5%.

Table 2.11

Static Analysis Results for the Pylon

	Case One	Case Two	Case Three
Von Mises Stress (psi) [1]	3590	9660	4900
Direct Shear Stress (psi)	49	168	61
Column Figure of Merit[2]	0.08	0.22	0.11
Buckling Flag	No Buckling	No Buckling	No Buckling
Angular Deflection (mrad)	1.46	3.80	2.14
Azimuth Twist (mrad)	0.09	0.30	0.45
Total RSS Deflection	1.46		

1. AISC allowable stress (Section 1.5 of Reference 5) = 49500 PSI
2. If the Figure of Merit is less than one, the column will resist bending and axial loading.

2.5.4.1 Integral Pylon Foundation Analysis

Past experience in the industry with array supports suggested that a single pier foundation was cost effective. Recent field experience and cost studies for heliostat supports (6) have shown the support pylon should be directly embedded into a vertical, cast in place pier. The embedded pylon tube was also designed to function as the concrete reinforcement. The heliostat designs required that the tube remain vertical while the concrete was poured and set. A leveling plate for the drive support was incorporated into the pylon design and will be implemented in Phase II. The leveling plate will reduce the required vertical tolerance of the pylon.

The alternate design was a cast-in-place pier with a reinforcing cage of re-bar embedded in it. Cast-in-anchor studs in the top surface of the pier would match a drilled flange welded to the bottom of the above ground portion of the support pylon. The cost of the flange fabrication, welding, re-bar cage, and anchor bolt placement was greater than the cost of the extra pylon support tube material.

For a multiple array installation, small cost savings are multiplied many times over. A rigorous and optimized foundation design is appropriate. An optimized design requires a test bore and local soil properties measurements to be made. The measured values are then used to calculate foundation strength and stiffness.

During Phase I activities, SKI chose a second approach for foundation design. Several empirical formulas have been developed in various industries that give

conservative and reliable pier sizes. Although a deeper hole and possibly a greater diameter pier was developed using the empirical approach, this did not add significant cost when only a few piers were being installed. The mobilization cost of the drilling truck and concrete delivery truck was greater than the cost of job site time and materials.

The analytical solution for sizing a rigid pier relates the pier depth, pier diameter, and soil bearing capacity to overturning moment. It is assumed that the pier does not deflect significantly. Defining the soil load bearing capacity is the most difficult part. An experienced construction engineer observed that for our soil a conservative value would be 200 lb/sq.ft. Handbook values showed a typical capacity of approximately 300 lb/sq.ft. for similar soil, confirming the conservative nature.

An engineering "rule-of-thumb" in the construction industry for piles is shown below as method A. Application of this formula to a dish support foundation, when compared to a rigorous analysis, showed a difference of only 10%. A reference book (Ref. 5) solution to pier sizing is shown below as method B.

Method

A $$\text{Force} = \frac{(\text{Depth}^3 * \text{Diameter} * \text{Allowable Soil Pressure})}{(12 * \text{Height})}$$

Method

B $$\text{Force} = \frac{(\text{Depth}^3 * \text{Diameter} * \text{Allowable Soil Pressure})}{(2 * (\text{Height} + \text{Depth}))}$$

The values used for sizing the 2 kW PV array foundation were as follows:

Height	8.5	feet
Diameter	1.5	feet
Force	1240	pounds
Allowable Soil Pressure	200	lb/sq.ft.

RESULTING DEPTH

Method A	8	feet
Method B	5	feet

A pier depth of 10 feet was specified for the actual installation. The eighteen-inch diameter pier was selected to readily accommodate the 8.625-inch diameter pylon tube.

2.5.4.2 Support Pylon Vibration Analysis

The natural frequency of the support pylon was calculated using simple spring-mass models (10) of the two different array orientations involved with the three design cases. These simple models of the tracker were used to make an estimate of the array's fundamental frequency. Past experience has shown that to avoid system excitation from the wind the natural frequency of the system cannot be less than one Hertz. The array was modeled as a mass; the pylon as a spring load in bending for the 27 mph and 50 mph array orientations (point mass model). The rotational vibration mode (disc spring model) was considered for the 90 mph stowed condition. The results of these two calculations indicated that the natural frequency, as modeled by the point mass-spring configuration, was approximately 5.4 Hz. The disc-spring model predicted an approximate natural frequency of 4.0 Hz.

2.5.5 Tracker Controls

The tracking control scheme used for the 2 kW SKI tracker is an open loop design. Position feedback signals were not generated by shadow-band sun sensors, but rather by optical incremental encoders mounted at each tracking axis. The desired tracker position for each axis was provided by an ephemeral calculation based on two algorithms. The first was a sun pointing program by J. Pacheco and Dr. D. Alpert of SNL National Laboratories (11). The second were the equations presented by Duffie and Beckman for the transformation of standard time to mean solar time (12). Tracking updates were then accomplished by comparing the error between the desired calculated tracker position and the actual encoded tracker position.

Calculation of the sun's position and the inherent tracker control logic were performed by an industrial programmable logic controller (PLC). The decision to utilize a PLC and not one of the current developed tracking controllers was based on availability and reliability. The PLC chosen by SKI was the Modicon Compact-984. This PLC was available worldwide, had a professional technical support team, and had been packaged to withstand the rigors of an industrial environment.

The Heliostat Az/El tracking program of Pacheco and Alpert was originally written in Fortran (11). The Fortran code was translated to the PLC's symbolic ladder logic format. These sun pointing computations were accommodated by the Modicon Compact-984 because this PLC had the ability to perform the floating point trigonometric calculations. The translated ladder logic program consisted of eight major routines that executed the required sun position calculations and provided the necessary interrogation and control of the tracker's input and output signals.

2.5.5.1 Hardware Description

The Modicon Compact 984-145 had 16K of user memory and scanned control logic at 4.25 msec per thousand logic words (one word is 2 bytes). The control inputs were addressed by the Modicon DEP-216 Input module. This unit provided 16 points of discrete, optically isolated 24-VDC input signals with a response time of 4 msec. After the program logic was solved, control signals were transmitted to the Modicon DAP-208 output module, which provided 8 relay contacts. The DAP-208 response time was 10 msec.

The Modicon PLC, I/O modules and a power supply were interfaced with each other via a common back plane. This arrangement allowed easy component replacement of any of the Modicon units. The back plane was a DIN rail mounted within a NEMA-4 enclosure. The input and output terminal blocks and the mechanical switching necessary for manual control of the tracker's speed and direction were also located in this enclosure. KBCC-125R DC motor controllers were mounted in a separate NEMA-4 enclosure to avoid RFI/EMI interference.

The azimuth axis limit switches allowed the tracker to rotate more than 360 degrees. The tracking envelope defined by the elevation limit switches was 100 degrees. Placement of the azimuth axis proximity switch gave an encoder initialization value and a stow position of 270 degrees. The elevation proximity switch was positioned to initialize the encoder and stow the tracker at 90 degrees.

The sign convention used for control software was that azimuth due north was equal to 0 degrees with positive travel clockwise. Zero degrees in elevation occurred when the array was perpendicular to the ground with positive travel counter-clockwise. The tracker array was parallel to grade with the lenses face up during stow.

The elevation and azimuth encoders (Heidenhain ROD-446) were positioned at the output side of their respective drive trains. This position eliminated errors from backlash in the azimuth gearbox and non-linearities from the elevation jackscrew being transmitted to the encoder. Azimuth position feedback was accomplished by shaft mounting the encoder directly to the output shaft of the azimuth gearbox. The resolution of the azimuth encoder was 0.436 mrad. The elevation encoder was interfaced with the elevation axis via a friction wheel. With consideration of the ratio between the wheel diameter and the elevation axis diameter, the elevation encoder's resolution was 0.30 mrad.

2.5.5.2 Software Description

Eight major routines were required for the SKI tracking control software. The first routine provided the time, date, declination angle, and hour angle. Second, the daily azimuth and elevation tracker positions were calculated. The third routine read and manipulated the square wave pulse train from the azimuth and elevation encoders. The fourth routine monitored all of the input sensors and

directed logic flow to the other routines. The command to initialize encoder position and move from stow were provided by the fifth routine. The translation of sun-to- tracker position was generated by the sixth routine. Commands to move to stow were provided in the seventh routine. Finally, the last routine was shared by the wake up, the sun tracking, and stow routines. This eighth routine controlled the motor drive outputs of speed, direction, and braking.

The Modicon PLC sequentially scanned the entire program in 8.5 msec. This scan time defined the rate at which the PLC accepted sensor inputs and changed controller outputs. The fourth routine of the SKI code decreased the scan time by skipping those routines that were not necessary for a unique tracker function (e.g. the sun tracking routine and the stow routine were not read while the tracker was being initialized). In order to provide a degree of confidence against PLC signal saturation, the maximum design signal input rate was 17 msec.

2.5.5.2.1 Segment One: Time, Declination Angle, Hour Angle

This segment was continuously scanned without interruption. It provided a correction for leap year and transformed the PLC clock format of HR:MIN:SEC to the required software format of SEC. The routine also calculated the solar time with respect to the local longitude, the standard meridian for the local time zone, and the equation of time (12). Finally, segment one defined the time increment for the declination and hour angle calculations at the local latitude with the method defined by Pacheco and Alpert (11).

2.5.5.2.2 Segment Two: Sun-Position Calculation

This segment was continuously scanned without interruption. It calculated the azimuth and zenith angle of the sun. These sun-position angles were transformed into the proper tracker coordinates to give the required azimuth angle and elevation angle of the tracker. The software was assumed that the tracking structure was perfectly aligned. The elevation axis was coincident with the gravity vector, and the azimuth axis was orthogonal to the elevation axis. The elevation and azimuth angle for solar noon and sunrise was also calculated by this routine before the current tracking day.

2.5.5.2.3 Segment Three: Encoder Sampling

This segment was continuously scanned without interruption. The quadrature square wave pulse train signal from both the azimuth and elevation axis encoders were processed by this routine. This information provided the controller with the position and travel direction of the tracker. Counting the pulse train from the respective encoders was a relatively simple procedure. However, determining the tracker's direction presented some challenges.

Ua1 and Ua2 represented the set of signals received by the DAP-216 input module. The control logic recognized clockwise rotation if signal Ua1 lagged

signal Ua2 and counter-clockwise rotation if Ua1 led Ua2. However, the encoder position counters did not begin updating until the tracker direction was determined. This caused the program to skip the initial position counts. The encoder counters were adjusted for missed counts each time motion started or when the tracker drives were reversed.

The calculated elevation and azimuth angle were converted to encoder counts and resolution with a scaling factor. The calculated resolution exceeded the encoder resolution (0.30 mrad for elevation, 0.44 mrad for azimuth). The scaling factors were 3294 for elevation, and 2292 for azimuth.

The elevation counter subtraction results were absolute value differences. Therefore, 5 degrees was added to the calculated elevation angle so that the negative counts would not be lost or interpreted as positive counts. When the elevation encoder count was initialized, the counters' value were set to 95 degrees to represent a physical tracker elevation position of 90 degrees

The azimuth encoder counter did recognize the appropriate sign of subtraction results. Therefore, the azimuth encoder count represented the tracker's physical azimuth position. The azimuth encoder was initialized to a value representing 270 degrees, and the tracker was physically at 270 degrees azimuth.

The azimuth travel exceeded 360 degrees. Consequently, the controller had to account for a singularity point at 0 degrees in the azimuth axis. The SKI tracking control software accomplished this task by resetting the azimuth encoder value based on the direction of travel in accordance with the tracking motion. For clockwise travel, the encoder count value was reset to 0 degrees. Conversely, when tracking counterclockwise, the azimuth encoder count was reset to 360 degrees.

To control excessive hunting in both axes, a user-specified deadband was added to both sides of the encoder count. One elevation count was equal to 0.30 mrad, and one azimuth count was equal to 0.436 mrad. Two counts were added and subtracted from both the elevation and azimuth count. This yielded an elevation encoder deadband of 0.60 mrad and an azimuth encoder deadband of 0.872 mrad.

The quadrature signals from the encoders had an edge separation of 1.7 microsecond per 100 kHz. In other words, if the encoder shafts were moving at a rate of 100 kHz (electrical), the signals coming into the input module would be 1.7 microseconds apart. The design scan rate of the PLC was 8.5 msec. Therefore, the maximum allowable rpm of either axis was 0.167 rpm. This limit provided a margin of safety of two against PLC signal saturation and prevented counting errors in the encoder software counters.

2.5.5.2.4 Segment Four: Main Program

This segment was continuously scanned without interruption. All position limit switches, the ambient light switch, and the wind velocity switch were monitored

in this program segment. The tracker moved to the stow position when these switches were activated. The stow command was immediate in response to limit switches and the wind switch. A 30-minute delay was provided when the ambient light fell below a user-specified threshold. This delay prevented excessive cycling on overcast days. The combined wind velocity (mean velocity plus gust) switch set point was 27 mph. The tracker was not returned to active status until the stow routine was completed.

In active status, the tracker checked all position and environmental sensors. If the conditions were acceptable, and the time of day fell between sunrise and sunset, the program logic flow was routed to the sun tracking routine of segment six.

2.5.5.2.5 Segment Five: Wakeup Routine

This routine was scanned conditionally. The program logic in this segment was operational only when the tracker was active. When the array was initialized, the encoder values were updated to the stow position count. The tracker was subsequently driven to the required azimuth and elevation angle.

The first step in initialization was to establish the azimuth reference point. A proximity switch target was attached to the pylon and aligned at 270 degrees. The software sent a motor drive signal to segment eight so that the tracker moved counterclockwise off of the target edge. The tracker immediately reversed direction (cw) when the proximity switch no longer sensed the target edge. During clockwise travel, the proximity switch reacquired the target edge. All azimuth tracker motion was subsequently stopped, and the azimuth software encoder counter was set to a value representing 270 degrees (10800 counts). The tracker was then allowed to move to the correct sun tracking azimuth position. Further azimuth updates were not allowed until the sun tracking routine was activated.

The elevation encoder reference point was established in the same fashion. The elevation proximity switch target was aligned at 90 degrees. The array moved clockwise, reversed direction when the target was no longer switched, and traveled until the target was reacquired. Elevation motion was temporarily stopped, the elevation encoder counter was set 95 degrees, and the tracker was allowed to move to the correct sun tracking elevation position.

The initialization routine was disabled, and program control was passed to the sun tracking routine (segment six).

2.5.5.2.6 Segment Six: Sun Tracking

This routine was scanned conditionally when the time of day corresponded to daylight hours and the initialization routine was complete. The first sequence positioned the tracker if the sun moved north of the zenith. This anomaly would occur when the tracker was installed at locations between the tropics. Because the elevation operational envelope was limited to 90 degrees, the tracker must

be spun 180 degrees about the azimuth axis for an "over the shoulder" sun tracking capability. First, the elevation angle at solar noon was checked to verify if its value was within 0.1 degree of 90 degrees (user specified range). Second, the time of day was checked to verify if its value is within 30 seconds of solar noon (user specified range). The tracker was moved at high speed about the azimuth axis until the 270 degree stow/encoder proximity switch was activated when both conditions were true. The routine continued normal sun tracking operation after the azimuth spin move was completed.

For normal sun tracking, updates of the tracker's elevation and azimuth axis during normal sun tracking were dependent on the error between the calculated and the actual encoder count. The maximum tolerated elevation error, or deadband, was defined as 0.60 mrad in elevation and 0.72 mrad in azimuth. The array was driven to the middle of the deadband range when updates were required.

2.5.5.2.7 Segment Seven: Stow Routine

This routine was scanned conditionally based on the sensor input status of segment four. The direction to stow for the elevation axis was always known based on the encoder count. The azimuthal direction during a drive to stow remained unchanged unless the limit switch at the end of travel was encountered. Limit switches automatically reversed the drive direction. This segment was active only during the drive-to-stow.

2.5.5.2.8 Segment Eight: Motor-Drive Routine

This routine was continually scanned without interruption. Its function was to energize the controller outputs determined by the parameter status of the three tracker- drive routines (wakeup, tracking, and stow). The outputs were:

- Azimuth motor on/off,
- Elevation motor on/off,
- Azimuth travel cw/ccw,
- Elevation travel cw/ccw,
- Azimuth motor speed low/high, and
- Elevation motor speed low/high.

All of these outputs were also available in manual control from switches mounted on the PLC enclosure.

2.5.6 Tracking Error

Four different errors contributed to the overall estimated tracking accuracy of the prototype 2 kW array: the PLC clock error, the errors due to the approximation of the sun's calculated position, the user-specified tracking deadband, and the

structural deflections of the tracker. The Modicon Compact-984 published clock accuracy was 16 sec per day (0-60 degrees Celsius). This PLC clock error would result in erroneous calculated sun positions.

The sun's position changed at a rate of 0.25 degrees per minute. Using a PLC clock error of 16 sec per day, the resulting pointing error was 1.152 mrad/day. The maximum pointing error would occur on June 21 when the length of the day was the longest (approx. 50436 sec.). In the Dallas area (latitude = 32 degrees), this pointing error was to be equal to 1.152 mrad/day * 1 day/86400 sec * 50436 sec = .672 mrad.

The equations used to calculate the daily position of the sun were based on the trigonometric relations used to compute Heliostat Az/El tracking positions. Approximations for the mean solar time were taken from the equations given by Duffie and Beckman (12). The precision of these equations to an accepted standard was not known. However, these equations had been used and presented by professionals in the solar field. Therefore, the approximations of the sun's position were considered appropriate for prototype tracking controls development.

The last two areas, which contribute to the total array tracking error, were those that involve the control deadband and the tracker's structural deflections. The user-specified deadband contributed 0.872 mrad error in azimuth and 0.60 error mrad in elevation. The total value of the tracker's structural deflection (27 mph wind) was 2.05 mrad.

The design goal for the total tracking error was 5 mrad. Error contributions from the above four categories were the following:

1. PLC clock = .672 mrad,
2. Sun-Position Calculations = n/a,
3. Deadband = 1.06 mrad, and
4. Structure = 2.05 mrad.

These individual deviations gave a total estimated tracker error of 3.782 mrad, which was 24.3% less than the tracker error design goal.

2.5.7 Prototype Costs

Unit construction costs for the tracking structure and the installation costs of the tracking controls were compiled for future comparison to similar systems. The construction cost of the tracker was the summation of the fabrication cost for each of the three subassemblies. These individual costs are summarized in Table 2.12. The tracking controls' costs are summarized in Table 2.13.

Comparisons to previous tracking systems were not made with respect to the costs of structure fabrication. However, a cost comparison was made with the

SolarTrak controller marketed by Solar Technologies Inc., Ltd. of Inglis, Florida. This comparison included only the cost of the controllers and their respective data manipulation interfaces. Peripheral sensors and components were not considered because these items were not unique to either control system. The control costs and the equipment included in the comparison are tabulated in Table 2.14.

Table 2.12

SKI Tracker Cost

Item	Cost
1. Module Frames Torque Tubes	$ 3,695.00
2. Az/El Drive Stage	$ 4,500.00
3. Pylon	$ 1,200.00
4. *Installation Assembly	$ 1,300.00
TOTAL	**$10,695.00**

*Does Not Include Cost of SKI Labor.

Table 2.13

SKI Controls Cost

Item	Cost
1. PLC I/O Modules, Associated Hardware	$ 903.00
2. DC Motor Controllers	$ 402.00
3. Sensors	$1,225.00
4. DC Motors	$ 327.00
5. Drive Train (AZ EL)	$2,212.00
6. Data Panel	$ 450.00
7. Misc. (Enclosures, Switches, etc.)	$ 756.00
TOTAL	**$6,275.00**

From the table, the cost of the PLC and its associated hardware showed an increase of 26.4% over the price of the SolarTrak controller.

However, the SolarTrak was not a commercially available controller within Phase I activities. Based on this information, SKI made the decision to design and fabricate its own controller. Components were of a proven design and had years of demonstrated performance in the field. Technical support and parts had worldwide availability. The total cost of the 2 kW tracker, considering structural, drive, and tracking controls, was equal to $16,970.00

Table 2.14

Controls Cost Comparison

Item	Cost
SOLARTRAK Controller	$ 650.00
SOLARTRAK User-interface	$ 420.00
TOTAL	**$1,070.00**
MODICON 984-130 PLC	$ 525.00
MODICON BDEP-216 Input Module	$ 120.00
MODICON BDAP-208 Output Module	$ 135.00
MODICON Primary Rack	$ 123.00
Quartech Data Panel	$ 450.00
TOTAL	**$1,353.00**

3.0 Phase II Results

The work completed during Phase II up to the date of the contract cancellation is summarized in Section 3.0. The summary includes discussions on the cell assemblies, the solder development, and tracker platform installation.

3.1 Cell Assemblies

Approximately 1000 cell assemblies had been made by SKI through the duration of this contract; these assemblies were divided into four major groups:

- Series 6-13: Preliminary experiments were made without pretinning the cell or spreader. Joints made during this phase were not successful;
- Series 14-21: A set of experiments on pretinning approaches was conducted. Cells made at the end of this set showed promise for good initial bond quality;
- Series 22-29: Refinements in the pretin and reflow process along with tool modifications were made; and
- Series 30-42: Several hundred cell assemblies were made to improve the repeatability of the complete solder process. The only process changes

made were the use of a solder paste to attach both the front and rear contacts and insuring that soldering occurred immediately following component cleaning. The final 444 cell assemblies made in this series demonstrated an excellent initial bond quality with repeatability. One cell assembly was rejected because of a electrical short; less than 7% (29) of the assemblies were rejected based on ultrasound imaging.

3.2 Solder Development

The solder development section summarizes the results from the solder testing regiment and the work that was scheduled to be performed during Phase II.

3.2.1 Test Results

SKI sent cell assemblies to SNL for electrical characterization and thermal cycling. Although one or two assemblies in samples of four or five had small (<10%) increases in void areas after 250 thermal shock cycles, the mean of the assemblies had much greater increases. It was SKI's understanding that experiments conducted by Tom Hund of SNL had shown similar results: individual assemblies survived, but the average degradation was too great to meet the evaluation test criterion.

Tom Hund suggested that the metallization failure in ASEC cells may have been responsible for the increase in void areas after cycling.

Experiments conducted by SNL on cell assemblies fabricated by SKI had clearly demonstrated this type of failure (metallization) in ASEC cells after humidity during Phase I. Galvanic corrosion had been suggested as a possible mechanism.

3.2.2 Further Solder Development

SKI intended to continue cell assembly development to reduce the void increase typically associated with fatigue failure in soldered joints through:

- fabrication of assemblies with new ASEC cells (ASEC was going to alter the sintering temperature and metallization sequence in an attempt to improve soldering and metallization performance);
- change the solder alloy, including the addition of antimony, to improve the fatigue strength of the materials;
- incorporate a copper clad molybdenum substrate between the cell and heat spreader; and
- encapsulate the cell assembly after soldering.

The antimony addition and intermediate substrate were both suggested by Tom Hund and appeared in the literature as approaches to improve fatigue strength. Other alloys with fatigue strength and control over other conditions that affect fatigue strength were also to be considered.

Cell encapsulation development was also to be continued. It was not clear, based on data supplied by SNL, that encapsulation affected the thermal cycle fatigue resistance of the cell assembly, although performance in a humidity cycle may have been substantially improved. Consequently, the encapsulation program was to be continued in parallel with improvements in thermal fatigue resistance.

Assembly encapsulation was being pursued because our cell assemblies had not passed humidity cycle testing, wet insulation tests added by SNL to the evaluation requirements would almost certainly require encapsulation, and all of the technical staff at SNL had indicated that cell encapsulation would be required for environmental protection. SKI was to continue to pursue the epoxy encapsulant that was identified as a preliminary candidate, along with the silicones recommended by SNL. It was our intent to also evaluate encapsulation performed by vendors specifically in the optical or electronic coating business.

SKI had a concern that the addition of an encapsulation system, particularly an organic material, may initially improve the environmental and dielectric performance of the assembly at the expense of optical reliability. We requested that SNL provide us with any references or recommendations available on encapsulant candidates that had demonstrated an ability to retain dielectric and environmental barrier properties with optical clarity after low or high concentration ultraviolet exposure or other environmental conditions that occur in a photovoltaic module.

3.3 Tracking Platform

The 2 kW prototype tracker array developed by SKI in Phase I was installed in SKI's test site. The prototype included the concentrating module support frames, drive stage, and the array support pylon.

The support system required simultaneous tracking in two axes. Dual axis shadow band was rejected because of the potential problems when the sun's image was lost. Sun reacquisition with the trackers was complicated by requirements to update two axes by different and unknown amounts.

A microprocessor was added to the tracker platform to resolve the problems with continuous updates for two axes. Microprocessors capable of supplying information for tracker updates during requisition were easily programmed for an open loop tracking system with no shadow band trackers.

By the end of the contract, SKI had installed two Type-III modules on the tracking platform and was monitoring the performance of the platform.

4.0 Commercial Markets

SKI has identified solar photovoltaics (PV) as a technology of choice for a commercial product. The PV industry has grown at a rate of 30 % in recent years, and the technology has received acceptance in many markets. This

"solid state" device, which generates electricity directly from sunlight, has found many uses from powering hand-held calculators to remote facilities. The high cost of PV cell manufacturing has previously limited growth to areas with less desirable competitors, i.e., batteries, or more costly options such as remote sites that need power. Even so, growth has been steady due to reduction in the perception of technical risk, efficiency improvement, and cost reduction. The ultimate goal of PV products for utility use has not been achieved due to cost barriers. Now, however, with the ever increasing cost of new electricity generating capacity and the steady reduction in the cost of PV cells, SKI feels that an entry into this industry is appropriate. Based on fifteen years of related research and specific PV research experience, the company is uniquely qualified for such an undertaking. SKI proposes two product types: a line of simple flat panels and two concentrators. A small concentrator for residential and remote sites and a second, larger unit for electric utilities.

The earliest product to be introduced will be the "One Sun" panel that will compete directly with currently available panels. The typical panel is 2' x 4' and is rated at 80 watts. The wholesale price is nominally $450 or $5.60 per watt. Most panel fabricators purchase cells form one of several very competitive cell manufacturers and assemble the cells into a series string that produces 12 or 24 volts. Each PV cell produces a nominal 0.5 volts, and 24 are wired in a series to produce 12 volts. Depending on the size of the cell, several strings may be used in a single panel. Typical materials include a glass or plastic cover, cells and conductors, bypass diodes, a metal frame, and glass or plastic backing.

SKI has developed a number of such components and are qualified to design and develop a quality product. Flat panel fabrication equipment is commercially available and some will be purchased, however, SKI has the technology to fabricate much of the necessary equipment and tooling. This will result in a competitive advantage in cost of market entry. Investigation of current costs and prices indicates that such a product could be produced and sold at a reasonable profit. The "One Sun" should receive ready market acceptance in view of SKI's award winning track record. A portion of the proceeds of the contemplated offering will be used to acquire equipment and develop the "One Sun" PV panel for sale to remote power producers, avant-garde home owners, and system integrators.

Two sizes of the PV concentrator array will be developed. The smaller of the two will be rated at 1 to 3 kilowatts. A tracking unit, called an array, is made up of a support structure, electromechanical drives, and number of modules. Each module will contain 24 small, high quality PV cells and an equal number of acrylic Fresnel lens each about seven inches square. The lens parquet will be retained by an aluminum housing in which the cells are located and protected from the weather. Each module of 2 x 12 lens/cell units will produce a nominal 100 watts (1/10 kilowatt). One array with 25 modules would measure approximately 15 feet square and produce enough electricity for a typical household. A larger unit in the range of 10-25 kilowatts will be developed for

electric utility applications. The modules are planned to be identical for both units.

Using a simple microprocessor and small electric motors, the array tracks during the day pointing all the lens directly at the sun. Each Fresnel lens concentrates the sun to a spot about one-half inch in diameter. A small secondary mirror is placed above each cell to catch any spillage and spread the solar energy uniformly over the cells active area. Each cell is bonded to a copper heat spreader that is bonded to the aluminum housing. The cell operates at about 30% efficiency rejecting the balance of the energy as heat by way of the copper heat spreader and the housing. After optical and electrical losses, the array is expected to operate at better than 20% efficiency (solar to electric). Levelized cost of electricity from the concentrator is expected to be below 20 cents per kWh initially, falling to 10 cents as production increases. The following discussion considers market potential and cost.

It is generally agreed in financial circles that an investment delivering 15% internal rate of return (IRR) is moderately attractive if the risk is understood and limited. If one assumes that return as a minimum and makes assumptions as to solar resources and other cost, a price range can be calculated by considering efficiency, value of product, state and local taxes, inflation, and O&M rates. Tables 4.1 and 4.2 show two calculations for 15% IRR for different assumed efficiency rates at an electric rate of $0.15/kWh. Figure 4.1 is a plot of array price verses annual efficiency at three estimated electric rates. The results are encouraging and suggest that initial sales may be made at prices above the DOE short-term goals.

Table 4.1 IRR Calculations Using 20% Efficiency

Analysis of Discounted Internal Rate of Return
For Small User Displacing Purchased Electricity

Assumptions:

Price / Sq M (installed)	536	$	Solar Annual	2.4	MWH/yr/sq m
Plant Life	20	Years	Annual Effic	20	%
Down Payment	536	$	Power Output	0.48	MWH/yr
Depreciation	7	Years	O&M Costs	3.33	% of Revenue
Federal Tax Rate	34	%	Parasitics $	0.15	$/kWh
State Tax Rate	9.6	%	Parasitic	0.72	%/yr
Note Amortization	15	Years	Yr 1 Elect $	0.15	$/kWh
Interest Rate	12	%	kWh Es Rate (1)	0.07	%/yr
Annual Debt Service	0		Inflation Rate (2)	0.03	%/yr
Discount Rate	0.15				

(1) Applies for 10 years, inflation thereafter
(2) Applies to O&M, Fuel, Electricity after 10 years
(3) Ignores loss carry forward

No Equity Case

Year of Operation	1	2	3	4	5	6	7	8	9	10-20
Electricity Savings	72.00	77.04	82.43	88.20	94.38	100.98	108.05	115.62	123.71	1695.35
Depreciation	-76.56	-76.56	-76.56	-76.56	-76.56	-76.56	-76.56			
Interest on Note	0.00	0.00	0.00	0.00	0.00	0.00	0.00	0.00	0.00	0.00
O&M Cost	-2.40	-2.47	-2.54	-2.62	-2.70	-2.78	-2.86	-2.95	-3.04	-40.07
Parasitic Cost	0.72	0.74	0.76	0.79	0.81	0.83	0.86	0.89	0.91	12.05
Property Tax @1.25%	-6.70	-6.70	-6.70	-6.70	-6.70	-6.70	-6.70	-6.70	-6.70	-73.70
Taxable Savings (3)	-12.95	-7.96	-2.62	3.10	9.22	15.77	22.78	106.85	114.88	1593.63
Federal Tax	0.00	0.00	0.00	-1.05	-3.13	-5.36	-7.74	-36.33	-39.06	-541.83
State Tax	0.00	0.00	0.00	-0.30	-0.88	-1.51	-2.19	-10.26	-11.03	-152.98
Principal Payment	0.00	0.00	0.00	0.00	0.00	0.00	0.00	0.00	0.00	0.00
Cash Flow	63.62	68.61	73.95	78.32	81.77	85.46	89.42	60.27	64.79	898.80
Discounted Cash Flow	63.62	59.66	55.92	51.5	46.75	42.49	38.66	22.66	21.18	134.06
NPV of Cash Flow	536.48									
Beginning Principal Bal	0.00	0.00	0.00	0.00	0.00	0.00	0.00	0.00	0.00	0.00

Table 4.2 IRR Calculations Using 14% Efficiency

Analysis of Discounted Internal Rate of Return
For Small User Displacing Purchased Electricity

Assumptions:

Price / Sq M (installed)	376	$	Solar Annual	2.4	MWH/yr/sq m
Plant Life	20	Years	Annual Effic	14	%
Down Payment	376	$	Power Output	0.336	MWH/yr
Depreciation	7	Years	O&M Costs	3.33	% of Revenue
Federal Tax Rate	34	%	Parasitics $	0.15	$/kWh
State Tax Rate	9.6	%	Parasitic	0.504	%/yr
Note Amortization	15	Years	Yr 1 Elect $	0.15	$/kWh
Interest Rate	12	%	kWh Es Rate (1)	0.07	%/yr
Annual Debt Service	0		Inflation Rate (2)	0.03	%/yr
Discount Rate	0.15				

(1) Applies for 10 years, inflation thereafter
(2) Applies to O&M, Fuel, Electricity after 10 years
(3) Ignores loss carry forward

No Equity Case

Year of Operation	1	2	3	4	5	6	7	8	9	10-20
Electricity Savings	50.4	53.93	57.70	61.74	66.06	70.69	75.64	80.93	86.60	1186.77
Depreciation	-53.71	-53.71	-53.71	-53.71	-53.71	-53.71	-53.71			
Interest on Note	0.00	0.00	0.00	0.00	0.00	0.00	0.00	0.00	0.00	0.00
O&M Cost	-1.68	-1.73	-1.78	-1.83	-1.89	-1.95	-2.00	-2.06	-2.13	-28.03
Parasitic Cost	0.50	0.52	0.53	0.55	0.57	0.58	0.60	0.62	0.64	8.93
Property Tax @1.25%	-4.70	-4.70	-4.70	-4.70	-4.70	-4.70	-4.70	-4.70	-4.70	-51.70
Taxable Savings (3)	-9.19	-5.70	-1.96	2.04	6.33	10.91	15.82	74.79	80.41	1115.44
Federal Tax	0.00	0.00	0.00	-0.70	-2.15	-3.71	-5.38	-25.43	-27.34	-379.20
State Tax	0.00	0.00	0.00	-0.20	-0.61	-1.05	-1.52	-7.18	-7.72	-107.08
Principal Payment	0.00	0.00	0.00	0.00	0.00	0.00	0.00	0.00	0.00	0.00
Cash Flow	44.53	48.02	51.76	54.87	57.28	59.87	62.64	42.18	45.35	629.10
Discounted Cash Flow	44.53	41.76	39.14	36.08	32.75	29.77	27.08	15.86	14.83	93.82
NPV of Cash Flow	375.59									
Beginning Principal Bal	0.00	0.00	0.00	0.00	0.00	0.00	0.00	0.00	0.00	0.00

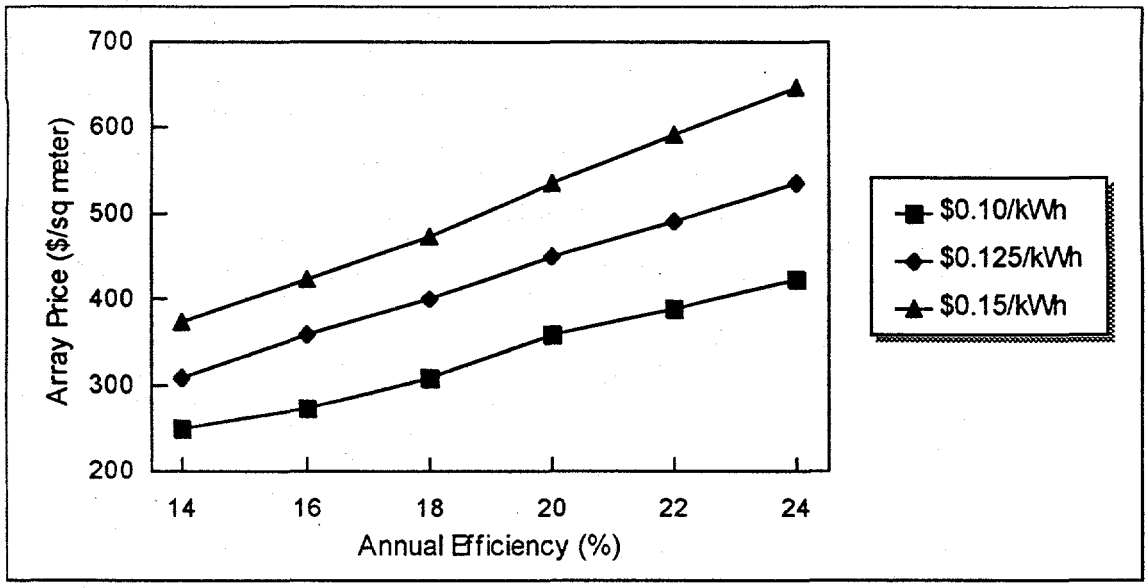

Figure 4.1 Array Price per Square Meter at 15% Internal Rate of Return

Realistically, during product concept introduction period, perception of risk dominates the decision making process; so simply making it to the DOE near-term cost goal or some IRR will not guarantee sales, not to mention profits. Profit is what is needed to produce Return on Investment on the investment that SKI is proposing herein, not to mention the investment that will be required in the commercialization period. If one calculates the sales volume in the first several years necessary to deliver a decent return on equity, the numbers are too optimistic. On the other hand, small business entrepreneurs often violate such financial guidelines and invest in the longer term. SKI has a history of building on sales rather than building a sales machine. That will be our primary plan.

4.1 Marketing Plan

The planned scenario includes a four-year market penetration. Initial sales will be subsidized by the manufacturer to offset initial low volume and high costs. The initial target market is expected to include commercial users, military bases, third world village power, Pacific Island Utilities, and remote applications for utilities by independent power producers.

Many commercial firms have expressed interest in emerging energy technologies. Cost conscious manufacturers are always investigating ways to reduce the cost of operation or production. This attitude was discovered by SKI during the early 1980's when solar thermal technology was near-cost competitive. Such firms would consider marginally cost effective technologies in limited application to gain a data base of experience in order to be at the "cutting edge", or appear to be. In either case, the PV concentrator should provide the unique qualities necessary to prompt sales.

With the DOD's posture on cost-shared energy conservation projects, third party owners could install and operate mini-utilities on military bases sharing savings with the military. While the concentrator technology is not as mobile as flat plate PV, the same military requirements of independence and zero fuel consumption may apply to generate some sales. In past years, SKI has been asked by several non-US military groups to investigate stand alone solar thermal systems. The central power block scheme was always the final deterrent to such a system. The PV concentrator may find application in this area due to its modularity.

Third world village power applications are always a viable target for renewable energy power producers. Electricity costs are high and fuel sources are limited. Such applications, while very attractive, will probably not take place until the latter stages of market penetration. By the third or fourth year of the marketing plan, six to seven years of performance and O&M documentation will be available. Based on that experience, sales into the village market will be viable in view of the limited qualified maintenance resource.

Applications on the Pacific Islands should be part of the first wave of market penetration. There two basic reasons: current economics and future economics. The cost of electricity is currently high, and initial sales will be near cost-effective due to the high cost of high power production. The desire to avoid future high costs should motivate these utilities. Third party ownership may be attractive for initial multiple array projects. The solar resources are also attractive.

Pacific Gas and Electric (PG & E) has noted that the rural market served by the utility is growing. Current transmission equipment is not projected to handle the growth in these remote areas of California. The cost of new larger transmission lines is prohibitive. Remote power production facilities are being considered; and with environmental controls, the PV concentrator technology may find early applications with that utility. Whether utility owned or independently owned, the cost of construction will be gaged against the cost of transmission line replacement. This likely event could provide a transitory period for market development in the second to fourth year.

The single most difficult task in any business is predicting future sales. When there is a history of sales, there may be some basis for predicting future sales; but any prediction of future sales for a new product concept is hazardous. Nevertheless, some prediction of future sales and profits must be made in order to justify the required capital expenditure.

SKI proposes to be in a position to manufacture a minimum of 1,000 modules. Market analysis will be performed during the initial stages of commercialization. When target markets are identified, market development begins. This is simply the sales period when the customer base is educated about the product. Few sales are made during this period, which may last 6 months to a year. The sales effort is ongoing while innovative finance plans are investigated.

Since the PV concentrator is a new product concept, the most similar product currently being sold will be identified, and the market for the product addressed. The target price should be that which takes some sales from that marketplace. In this case, the flat plate PV system may qualify as the closest concept, but not necessarily.

The analogy of solar thermal flat plates versus tracking troughs could be made here. In our experience, a 25 % price advantage was enough to motivate a customer to undertake the risk of a complex tracking system over thermal flat plates. If that analogy holds true, the true short-term price goal will have been identified; but these decisions can only be made during and after the market analysis period when customers are interviewed directly.

As sales grow, the company will have, at hand, engineering plans for manufacturing processes and equipment. These plans can be immediately implemented as justified by cost reduction and increased productivity. The processes and equipment are envisioned to be as flexible as possible in order to be adaptable to design changes and sales volume variations. Robotics will play a major role in the process system. It should be noted that the company's entire lighting manufacturing division is exclusively C.N.C. and capable of any volume with minimum special tooling.

In order to make an estimate of the allowable capital investment, some assumptions could be made. If the equipment were amortized over seven years and the discount rate chosen is 15%, the investment per dollar in sales can be calculated.

Year	1	2	3	4	5	6	7
Sales	100	100	100	100	100	100	100
Profits @ 10%	10	10	10	10	10	10	10
NPV @ 15%	10	8.70	7.56	6.58	5.71	4.97	4.32

Total NPV = $47.84

Therefore for each $100 in sustained sales, an equipment investment of $47.84 could be made.

If arrays produce 120-170 watts per m^2, one megawatt per year would require between 4,000 and 6,000 square meters or 5,500 to 8,300 modules. That would translate to between 1.2 and 1.8 million in sales per year. Assuming the higher figure, one could estimate a potential for between $500,000 and $800,000 in capital investment.

Obviously, sales expense and other market development costs would lower that potential for investment by diluting the profit stream. Even though an estimate of

sales verses time made at this time is baseless, one must be made to give some idea to the reader of the investment potential faced by SKI.

Assumes 0.72 m^2 and 123 watts/module

Year	1	2	3	4	5	6	7
Modules	1000	4000	8000	12000	20000	40000	80000
M.W.	.12	.48	1	1.5	2.5	5	10
$/$m^2$	400	350	300	275	265	250	240
Profit (thousands)	29	115	232	348	580	1160	2320
NPV	29	100	175	228	331	576	1003
Sales Cost	(320)	(320)	(320)	(320)	(320)	(320)	(320)
NPV Sales Cost	(320)	(278)	(242)	(210)	(182)	(159)	(138)
Net NPV	(291)	(178)	(67)	18	149	417	865

Total NPV = 913

The foregoing calculation suggests that up to $900,000 could be invested if all assumptions are correct. Obviously, insufficient information exists to make any reasonable decisions as to investment. On the other hand, if equipment is purchased on an as needed for growth basis, decisions can be made on some reasonable basis.

5.0 Conclusions

The first phase in development of a point-focus concentrating PV module was a success. Cell assembly and module fabrication issues were addressed by utilizing cost-effective materials and defining low-cost manufacturing methods. Material costs were minimized, although processing and assembly cost evaluation were an ongoing task in the contract.

The module design was acceptable from a structural and heat rejection standpoint. Analysis and subsequent testing showed the thermal path from PV cell to the module housing was sufficient to maintain an acceptable cell operating temperature. Material costs were minimized by eliminating the need for complex heat dissipation devices or active cooling elements.

The changeover from two 2x6 Fresnel lens parquets to six 2x2 Fresnel lens parquets would decrease lens distortion and should result in better optical efficiency. Single lenses require machining prior to solvent bonding in a 2x6 parquet, but this was not the case for the 2x2 parquets. Therefore, fabrication

costs were lower in the 2x2 parquets. Molding forces and die size required for a 2x6 lens parquet made molding this as a single part impractical.

Cell assembly survival under accelerated environmental aging was considered a major objective of Phase I. Several months into Phase I, the cell assembly fabrication process was established, and these cell assemblies had only one weak link. This weak link was the aluminum metallization on the back of the PV cell structure under humidity/freeze cycling. Void ratio under the PV cell increased in every case during thermal and humidity/freeze cycling. However, cell assembly electrical performance had no significant decrease when thermal cycling alone was performed. Therefore, it is believed that the humidity/freeze cycle allowed moisture to be captured beneath the cell. Cycle time was insufficient to allow moisture beneath the cell to dissipate prior to reaching the freezing point. As the freezing moisture expanded, crack propagation occurred.

The module met or exceeded electrical performance expectations for the first phase. Efficiency losses due to the cell assembly and module fabrication tolerances were negligible. As lens optical quality increased and concentrating PV cell inefficiencies met their expectations, module efficiencies increased.

The water spray test of the module indicated several leak points. All of these leak points were apparently at the lens-to-housing lip interface. Leaks were not more prevalent in certain locations than others. The water path seemed to originate at small orifices around the edge and lens partition clips and travel to gaps and expansion slots in the Fresnel lens.

The SKI tracker design applied commercially available components in a simple innovative manner. The design may be readily scaled to larger arrays, such as a 10 kW tracker. Actuator backlash, tracker alignment, and deflection errors were controlled in the drive design. The design also permitted simple field servicing of all actuators, bearings, and sensors.

The tracker controller was versatile, easily serviceable, and has worldwide availability. Controller programming was easily modified since modifications of the software could be accomplished using a portable computer.

6.0 References

1. SKI, Commercial Photovoltaic Concentrator Module and Tracker Development - Phase I Final Report, Submitted to SNL June 1993
2. R. S. Barlow and E. H. Richards, "Qualification of Photovoltaic Concentrator Modules and Cell Assemblies, " SAND86-2743, Albuquerque, NM: SNL National Laboratories, January 1988
3. S. T. Saifee and G. Hutchison, Development of a Commercial Photovoltaic Concentrator Module. SNL 92-7001, Albuquerque, NM: SNL National Laboratories, March 1992.
4. M. L. Whipple, "Evaluation Test Report, SKI Cell Assemblies, Concentrator Initiative Contract 40-8941B, Phase I," May 22, 1992.
5. Manual of Steel Construction, 8th ed., American Institute of Steel Construction, Inc., 1980.
6. J. A. Peterka, J. J. Lou, and J. E. Cermak, Wind-Tunnel Test of a Photovoltaic Concentrator Array, CER78-79JAP-JJL-JEC62, Fort Collins, CO: Colorado State University, June 1979.
7. W. C. Young, Roark's Formulas for Stress and Strain, 6th ed., New York: McGraw-Hill, 1989.
8. J. E. Shigley and L. D. Mitchell, Mechanical Engineering Design, 4th ed., New York: McGraw-Hill, 1983.
9. F. P. Beer and E. R. Johnston, Jr., Mechanics of Materials, New York: McGraw-Hill, 1981.
10. E. A. Avallone and T. Baumeister III, Marks' Standard Handbook for Mechanical Engineers, 9th ed., New York: McGraw-Hill, 1987.
11. J. Pacheco and Dr.. D. Alpert, "Sun Pointing Program", personal correspondence to David L. White, Solar Kinetics, Inc, 1989.
12. J. A. Duffie and W. A. Beckman, Solar Engineering of Thermal Processes, John Wiley and Sons, 1980.

MS-0899
Technical Library
Org. 13414 (5)

MS-0619
Print Media
Org. 12615

MS-0100
Document Processing for DOE/OSTI (2)

MS-9018
Central Technical Files
Org. 8523-2

MS-0752
M. L. Tatro
Org. 6219

MS-0752
A. B. Maish
Org. 6219

MS-0753
C. P. Cameron
Org. 6218

MS-0702
D. E. Arvizu
Org. 6200

MS-0702
A. VanArsdall
Org. 6200

Mr. James Rannels, EE-131
Forrestal Building
U. S. Department of Energy
1000 Independence Avenue, SW
Washington, DC 20585

MS-0753
M. Valencia (5)
Org. 6218

Mr. Gus Hutchison (5)
Solar Kinetics, Inc.
10635 King William Drive
Dallas, TX 75220

Mr. Michael Pulscak, EE-131
Forrestal Building
U. S. Department of Energy
1000 Independence Avenue, SW
Washington, DC 20585

Mr. Thomas Surek
NREL
1617 Cole Boulevard
Golden, CO 80401